RADIOSENSITIZATION EFFECT OF ALPHA-MANGOSTIN ON CERVICAL CANCER (HELA) CELLS

Pimvaree Aissara

A Thesis Submitted to the Graduate School of Naresuan University

in Partial Fulfillment of the Requirements

for the Master of Science in Medical Physics

2025

RADIOSENSITIZATION EFFECT OF ALPHA-MANGOSTIN ON CERVICAL CANCER (HELA) CELLS

Pimvaree Aissara

A Thesis Submitted to the Graduate School of Naresuan University

in Partial Fulfillment of the Requirements

for the Master of Science in Medical Physics

2025

Thesis entitled " RADIOSENSITIZATION EFFECT OF ALPHA-MANGOSTIN ON CERVICAL CANCER (HELA) CELLS"

by Pimvaree Aissara

has been approved by the Graduate School as partial fulfillment of the requirements for the Master of Science in Medical Physics of Naresuan University

Oral Defense Committee

…….Chair

(Associate Professor Suchart Kothan, Ph.D.)

…….Advisor

(Assistant Professor Ausanai Prapan, Dr. rer. medic.)

…….Co-Advisor

(Assistant Professor Chanyatip Suwannasing, Ph.D.)

…….Internal Examiner

(Assistant Professor Thanyawee Pengpan, Ph.D.)

Approved

……

(Assistant Professor Chommanad Intajamornrak, Ph.D.)

Head, Department of Linguistics, Folklore, Philosophy and Religion, Faculty of Humanities

Acting Dean of the Graduate School

Title RADIOSENSITIZATION EFFECT OF ALPHA-MANGOSTIN ON CERVICAL CANCER (HELA) CELLS

Author Pimvaree Aissara

Advisor Assistant Professor Ausanai Prapan, Dr. rer. medic.

Co-Advisor Assistant Professor Chanyatip Suwannasing, Ph.D.

Academic Paper Master of Science Thesis in Medical Physics, Naresuan University, 2025

Keywords cervical cancer, Alpha-Mangostin, radiotherapy, radiosensitizer, G2/M arrest

ABSTRACT

Radiotherapy (RT) is a common treatment for cervical cancer, but its effectiveness is often limited by tumor hypoxia and low radiosensitivity. Radiosensitizers that improve RT without increasing the dose are therefore of clinical interest. Alpha-Mangostin (AM), a xanthone from Garcinia mangostana, has anticancer and ROS-increasing properties. This study evaluated whether AM enhances radiosensitivity in vitro. Cytotoxicity (0–35 μM) was measured by the MTT assay, and radiation sensitivity (0–6 Gy) was assessed through clonogenic survival. ROS detection assay, γ-H2AX immunofluorescence, cell cycle analysis, apoptosis measurement, and clonogenic survival tests were used to examine the radiosensitization effect. AM showed dose-dependent cytotoxicity in HeLa cells, with an inhibitory concentration 20 (IC20) of 13.67 μM, while sparing fibroblasts. The radiation lethal dose 20 (LD20) was 1.4 Gy. However, the combination treatment used AM at 12 μM (IC14) with 2 Gy (LD30) irradiation (IR) to avoid 50% cell death. AM increased G2/M arrest by 21.10% ($p < 0.01$) compared to controls. The combined treatment caused a 4.07-fold increase in oxidative stress relative to the control ($p < 0.0001$), which was higher than either AM alone or IR alone. Additionally, this combination increased γ-H2AX-positive cells to 48.2% ($p < 0.0001$), raised apoptosis to 39.48% ($p < 0.0001$), and reduced clonogenic survival to 28% ($p < 0.0001$) compared to RT alone. This resulted in a sensitizer enhancement ratio (SER) of 2.48. Therefore, AM effectively radiosensitized HeLa cells by increasing oxidative stress, promoting DNA double-strand breaks, and inducing G2/M arrest.

ACKNOWLEDGEMENT

The researcher would like to express her deepest gratitude to Assistant Professor Dr. Ausanai Prapan, Chairman of the Thesis Advisory Committee, and Assistant Professor Dr. Chanyatip Suwannasing, Member of the Thesis Advisory Committee, for their invaluable guidance, insightful advice, and continuous support throughout the entire period of this thesis research.

The researcher also wishes to express sincere appreciation to the Thesis Examination Committee, Associate Professor Dr. Suchart Kothan and Assistant Professor Dr. Thanyawee Pengpan, for their constructive comments and valuable suggestions, which greatly contributed to the successful completion of this thesis.

The researcher sincerely thanks the Faculty of Allied Health Sciences, Naresuan University, for generously providing laboratory facilities and institutional support essential for this research. Appreciation is also extended to the Department of Radiology, Faculty of Medicine, Naresuan University, for granting access to the linear accelerator (LINAC) facility. Special thanks are given to Ms. Kamonchanok Nobphuek, Medical Physicist, for her invaluable technical assistance with the irradiation setup.

Finally, the researcher would like to express sincere gratitude to all individuals who contributed to this thesis through their assistance, encouragement, and support. The researcher hopes that the knowledge and findings derived from this thesis will be valuable and beneficial for future research and practical applications.

Pimvaree Aissara

TABLE OF CONTENT

Page

LIST OF TABLES

Page

LIST OF FIGURES

Page

ABBREVIATIONS

AM	=	Alpha-Mangostin
HeLa	=	Human Cervical Cancer Cell Lines
G0/G1	=	Gap 0 and Gap 1
G2/M	=	Gap 2 and Mitotic phase
Gy	=	Gray
RT	=	Radiotherapy
IR	=	Irradiation
mL	=	Milliliter
µL	=	Microliter
MV	=	Megavolt
S	=	Synthesis phase
µg/mL	=	Micrograms per milliliter
SF	=	Survival Fraction
SER	=	Sensitizer Enhancement Ratio
ROS	=	Reactive Oxygen Species
µM	=	Micromolar
LD	=	Lethal Dose

CHAPTER I

INTRODUCTION

Background and rationale

Cervical cancer is the eighth most diagnosed cancer worldwide and the fourth leading cancer among women (1). In Thailand, it ranks as the second most prevalent cancer in women (2). Cervical cancer is caused mainly by a human papillomavirus (HPV) infection (3). Although cervical cancer death rates dropped between 1930 and 2012 due to early detection, the cancer remains a significant health risk. Statistics reveal that between 2012 and 2018, there was a significant rise in both the number of deaths and new cervical cancer cases worldwide. The primary variables influencing cervical cancer patients' mortality include recurrence and metastasis to other locations such as lymph nodes, lungs, and liver (4, 5).

Surgery is the common treatment for early-stage cancer. Additionally, chemotherapy and radiotherapy (RT) are used to treat advanced-stage cancer (6). RT is one of common methods used for the treatment of cancer by employing ionizing radiation to destroy cancer cells. However, resistance to RT, particularly in hypoxic (oxygen-deficient) tumors, can reduce treatment efficacy, and RT can cause injury to normal tissues surrounding the tumor (7, 8). Furthermore, chemotherapy is one of the standard cancer treatments that utilizes drugs with antineoplastic properties to inhibit tumor cell division and proliferation, helping prevent cancer invasion and metastasis. However, chemotherapy often causes severe side effects, including hair loss, nausea, and myelosuppression (bone marrow suppression). As mentioned above, combining a chemosensitizer or radiosensitizer with IR could be a promising approach to enhance therapeutic efficacy.

Currently, researchers are exploring natural compounds as chemosensitizers to improve treatment outcomes (9-11). Many natural compounds are under investigation for their potential as chemosensitizers and radiosensitizers in chemotherapy and RT (12, 13). For example, Chendil, D. et al. demonstrated that curcumin has radiosensitizing effects in prostate carcinoma cells by inhibiting NFκB and adjusting the Bcl-2:Bax ratio to promote radiation-induced apoptosis (14), Bola Sadashiva Satish Rao, et al. found that Plumbagin shows significant radiosensitizing activity in chemoresistant B16F1 melanoma cells through ROS-mediated DNA damage, cell cycle arrest at G2/M, and activation of the intrinsic apoptotic pathway, suggesting potential as a clinical radiosensitizer (15), Additionally, Yuan Shao. et al. demonstrated that Resveratrol exhibits radiosensitizing effects in FADU hypopharyngeal carcinoma cells by inducing apoptosis and perturbing the cell cycle (16). To address these challenges, both synthetic and natural radiosensitizers are being explored to improve the effectiveness of RT while minimizing side effects.

Alpha-Mangostin (AM), a key compound in the mangosteen peel (*Garcinia mangostana L.*), has a long history of use in traditional Thai medicine for treating skin conditions, wounds, and digestive issues. As a type of xanthone, AM is recognized for its antioxidant, anti-inflammatory, and anticancer effects (17). Studies have shown that AM increases reactive oxygen species (ROS) in cancer cells, which can lead to genetic damage and mitochondrial dysfunction, ultimately inducing apoptosis in various cancers like lung, breast, and cervical cancer. For example, in HeLa cells, AM treatment caused apoptosis marked by nuclear shrinkage, chromatin condensation, and formation of apoptotic bodies. Its mechanism involves activating caspase-3/7 and caspase-9, affecting mitochondrial membrane potential to release cytochrome C, triggering cell death (18-23). Research by El Habbash AI et al. also indicates that AM can halt the cell cycle at G2/M phase, thereby preventing cell proliferation (24).

Moreover, the anticancer properties of AM have been widely studied, although its use as a radiosensitizer has not been thoroughly studied. It is crucial to investigate whether it can increase the radiosensitivity of HeLa cells, as this might lead to more effective combination treatments. These treatments might enhance outcomes for patients with cervical cancer by decreasing the required radiation dose and reducing RT side effects.

This research hypothesizes that AM can increase the sensitivity of HeLa cells to radiation and, when combined with radiation, decrease survival rates more than radiation alone.

Objective

To investigate the radiosensitizing effect of AM in combination with IR on HeLa cells.

Research Scope

This thesis examines the radiosensitizing effect of Alpha-Mangostin (AM) on HeLa cells. Briefly, cytotoxicity is evaluated at various concentrations of AM, and the 20% inhibitory concentration (IC20) is determined using the MTT assay. To assess radiosensitization, the IC20 of AM is combined with radiation doses of 2 Gy delivered by a 6 MV linear accelerator (LINAC) to HeLa cells. The survival fraction (SF) and Sensitizer Enhancement Ratio (SER) are measured through clonogenic assays. Additionally, further experiments are conducted to evaluate apoptosis, cell cycle progression, immunofluorescence labeling, and ROS detection. Data is analyzed statistically with GraphPad Prism software, and all experiments are performed in triplicate and three independent times.

Research Hypothesis

AM increases the radiosensitivity of cervical cancer cells (HeLa), leading to a greater decrease in cell survival when combined with ionizing radiation compared to AM or radiation alone.

CHAPTER II

LITERATURE REVIEW

2.1 Cervical Cancer

Cervical cancer results from infection with human papillomavirus (HPV), a high-risk (oncogenic) strain. The most common strain is type 16, followed by 18, 31, 33, 45, 52, and 58. It is usually transmitted through sexual contact, with 90% of cervical cancers being squamous cell carcinomas and 10% being adenocarcinomas. When infected with HPV, the virus alters the genetic material in normal cervical cells, triggering a mechanism that causes uncontrollable cell growth, eventually leading to tumors. It can occur at any age but is more common in older individuals because HPV shows symptoms after infection persist for more than 5-10 years before progressing to cancer. Men infected with HPV can serve as carriers, transmitting the virus to women, and are also at risk of developing cancers of the penis and anus (25-27). HPV produces two main carcinogenic proteins, E6 and E7, which disrupt cell protein functions. The E6 protein interacts with E6-associated protein (E6-AP), an E3 ubiquitin ligase, and together they bind to p53, a tumor suppressor that controls cell division. This binding tags p53 for proteasomal degradation. When DNA damage or abnormalities occur, the depletion of p53 prevents cells from halting division, allowing continued proliferation. HPV can also promote the production of telomerase reverse transcriptase (hTERT), a component of telomerase. Telomerase extends telomeres at chromosome ends, enabling cells to divide indefinitely without aging or growth arrest. The E7 protein interacts with pRB and other family members, preventing pRB from regulating E2F transcription factors. E2F factors then promote gene expression necessary for cell division, enabling continuous cell proliferation (Figure 1) (28-32).

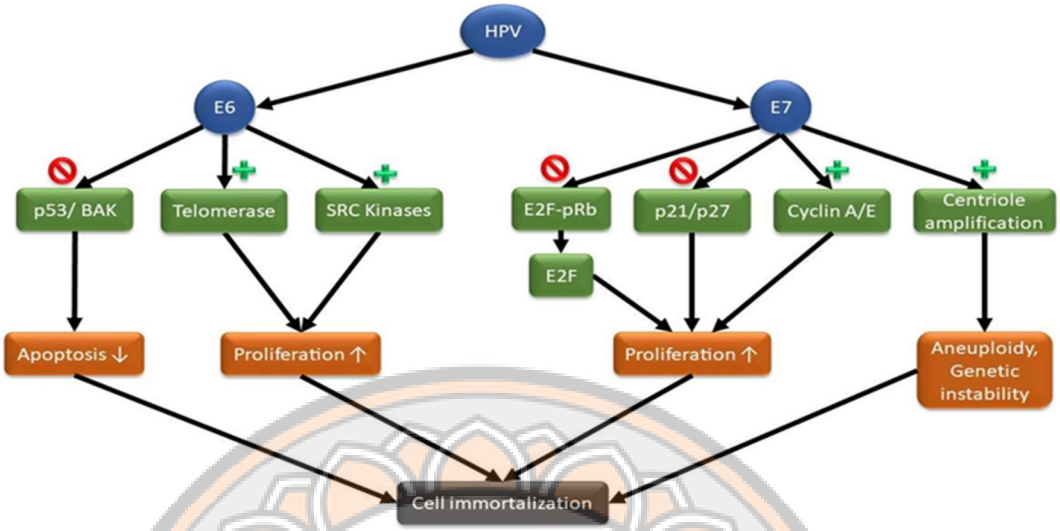

Figure 1 Molecular pathways affected by HPV-oncoproteins.

Source: Abboodi FF, Creek KE, Pirisi LA. Abstract LB-329: Molecular mechanisms of loss of E7 expression in HPV16-transformed human keratinocytes. Cancer Research. 2019;79

The cycle of cervical cancer starts with being infected with the HPV virus from a wound on the cervical lining. The HPV virus will enter the wound to the surface layer of the cervical lining (Transformation Zone) and increase the number of cells to the upper lining. This allows the virus to spread to other organs. This cycle lasts 10-20 years before the disease appears (33-35). When cervical cancer spreads, it will spread through various channels as follows: (36, 37)

1. Inside the cervix: caused by a small spot of cancer that has spread to the surrounding area until it spreads throughout the cervix, causing the cervix to become more significant (diameter greater than or equal to 8 centimeters), appearing as a wound or lump protruding or inserting into the cervical tissue.
2. Spread to nearby organs: Cancer will spread along the cervical tissue to nearby organs in all directions.
3. Lymphatic system: It usually starts from the lymphatic system in the pelvic area and spreads along the lymphatic vessels to the area above the left collarbone.
4. The bloodstream and lymph vessels eventually enter other organs, such as the liver, lungs, and brain.

Cervical cancer staging, according to the International Federation of Gynecology and Obstetrics (FIGO) system, is based on the size of the cervix and the spread to distant organs (Figure 2). It is divided into (38, 39)

1. Stage I: Cancer is still limited to the cervix.
2. Stage II: Cancer has spread to the upper vagina or adjacent cervical tissue but not to the adjacent pelvic wall.
3. Stage III: Cancer has spread to the lower vagina or all adjacent cervical tissue and to the adjacent pelvic wall.
4. Stage IV: Cancer has spread to distant organs.

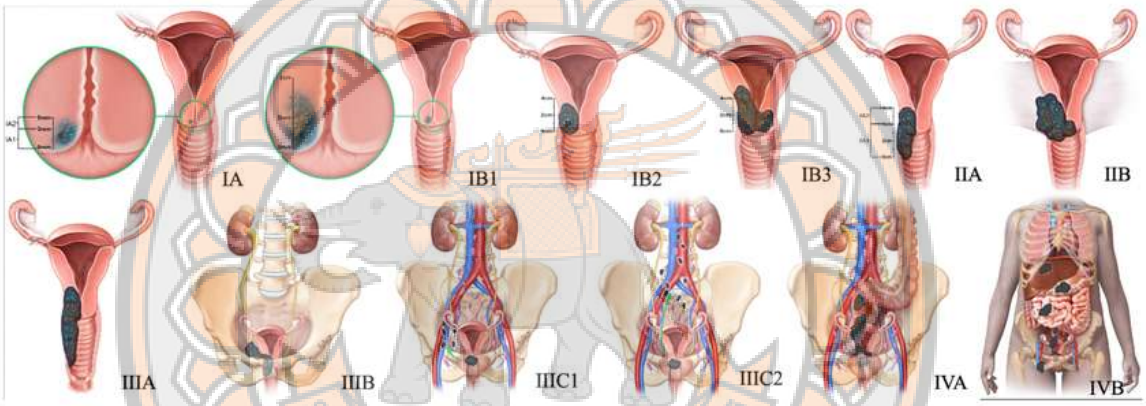

Figure 2 2018 FIGO staging system for cervical cancer.

Source: Virarkar M, Vulasala SS, Morani A, Waters R, Gopireddy D, Kumar S, et al. Neuroendocrine Neoplasms of the Gynecologic Tract. Cancers. 2022; 14:1835.)

2.2 Treatment of cervical cancer

Currently, the main treatment options for cervical cancer include surgery, chemotherapy, RT, and combination therapy, depending primarily on the stage of the cancer.

1. Surgery

   Surgery is a widely used and highly effective method for treating early-stage cervical cancer, as it directly removes cancerous tissue. It can also be used to remove tissue where cancer has metastasized. Currently, surgical procedures for cervical cancer treatment include total hysterectomy, radical hysterectomy, loop electrosurgical excision procedure (LEEP), conization, radical trachelectomy, and cryosurgery. The type of surgery is selected based on the stage of the disease and the extent of tumor spreading. Despite its high effectiveness, surgery has certain drawbacks. There may be side effects such as infection, blood loss, damage to nearby organs, blood clots, and radical hysterectomy performed laparoscopically, which has been associated with an increased risk of cancer recurrence, loss of fertility, and long-term urinary dysfunction (40-42).
2. Chemotherapy

   Chemotherapy is the mainstay of oncology treatment, with cytotoxic medicines used to target rapidly dividing cancer cells. The basic mechanism includes inhibiting cell division via multiple routes, including DNA damage, enzyme inhibition, and cell cycle disruption (43). These drugs work through the body, making them especially effective in treating metastatic cancer. Chemotherapy has proven its therapeutic efficacy, especially in blood malignancies like leukemia and lymphoma (44). Chemotherapy medicines can reach distant metastases due to systemic medication distribution (45). However, chemotherapy for cervical cancer treatment still has some important limitations. One issue is that chemotherapy is non-specific, affecting both cancer cells and quickly dividing normal cells, resulting in side effects that include bone marrow suppression, gastrointestinal damage, and hair loss (46). Furthermore, cancer cells develop drug resistance through various biological mechanisms, including increased drug excretion, modification of drug targets, and accelerated DNA repair, all of which face significant barriers to successful therapy (47).
3. Radiotherapy

   RT for cervical cancer can be classified into two types: external RT with a particle accelerator, which can treat the tumor and lymph nodes in the pelvis by modulating the radiation beam to increase precision and reduce side effects (48), and internal brachytherapy, which requires inserting a radiation source directly into the uterus or vagina. This method gives strong doses of radiation to be given directly to the tumor while reducing radiation exposure to surrounding tissues (49). However, RT has a few drawbacks, including the difficulty of cancer cells becoming radioresistant in a low-oxygen environment and requiring higher radiation doses to achieve the desired therapeutic outcome. Furthermore, side effects on normal surrounding tissues have been reported, such as bladder and

intestinal inflammation, vaginal strictures, and other long-term problems. However, indicating that while side effects may occur, they are frequently less severe compared to other treatment techniques (50-53).

Most cervical cancer therapies involve surgery and chemotherapy combined with RT. This is due to the ineffectiveness of a single treatment technique and the elevated risk of surgery and chemotherapy. As a result, RT is a viable alternative treatment since it is local and has fewer side effects than the two procedures mentioned above.

2.3 Effects of radiation on cells

When living cells are exposed to radiation, it affects biomolecules and organelles within the cell both directly and indirectly, including proteins, lipids, carbohydrates, mitochondria, and most notably, DNA. Radiation directly damages cell DNA, while indirect effects involve free radicals that also harm DNA. Generally, radiation causes more damage to DNA through indirect mechanisms than direct ones. This damage includes single-strand breaks, double-strand breaks, damaged bases, and DNA-protein cross-links. It also leads to cell abnormalities, which vary depending on the cell type, radiation dose, and radiation type. Cellular abnormalities and their features include:

1. Cells divide more slowly (division delay) or cease to divide (reproductive death) because of radiation damage to biomolecules, causing the functioning of those biomolecules to malfunction; for example, enzymes work less, leading to division reactions to decrease and causing cells to divide slower. If the genetic material (DNA) is damaged, the division process will slow down to repair the DNA. However, the cell will finally stop dividing if the DNA becomes so damaged that it cannot be restored.
2. Cell death during interphase. If cells are exposed to radiation and are irreparably damaged beyond repair, they will die without continuing to survive divide.
3. Cell death during mitosis. Radiation-damaged cells may proceed to the next phase of the cell cycle, but they will die upon reaching mitosis. This includes cells that have divided once or twice after radiation exposure. They will die during the next division because of genetic damage. In the fields of radiobiology, oncology, and research, there are two forms of cell death:

    3.1. In vitro: Dead cells will continue to seem normal, can produce proteins, and divide for another 1-2 cycles before becoming unable to divide further.

    3.2. Tumor Cells: Dead cells cannot divide again. And cannot spread (metastasize) farther.

The classification of cell death according to cell type is the following:

1. Differentiated cells, such as nerve cells, muscle cells, secretory cells, and so on, have evolved to execute specialized activities. They do not divide. When cells in this category die, it demonstrates they cannot complete their tasks or have lost their ability to function.
2. Proliferating cells, such as stem cells and the intestinal epithelium, represent cells that divide. Cells in this category die immediately and no longer divide. Cell death occurs when radiation causes damage to cells that cannot be repaired. The mechanism of cell death after radiation exposure is divided into four mechanisms as follows (Figure 3):

    2.1. Apoptosis is a programmed dying process in normal and abnormal cells. It is essential for life, as it supports various bodily functions, including proper cell turnover, healthy organ development, and immune system modulation. The features of apoptosis are as follows:
        1) It is a death caused by cellular self-destruction in eukaryotic cells.
        2) This is an ATP-dependent mechanism.
        3) DNA breaks at a certain size.
        4) There is no rupture of the cell membrane or inflammation.
        5) The cell is fragmented into smaller sections known as apoptotic bodies.

    2.2. Necrosis is a process of death caused by pathological circumstances such as toxin exposure or a lack of oxygen. Cells will enlarge, mitochondria will lose their function, and cell membranes will rupture, allowing internal cell components to escape into the extracellular area, causing inflammation and damage to surround tissues. DNA will be fragmented into uneven sizes, and ATP will be ineffective.

    2.3. Mitotic catastrophe is the death of cancer cells during the mitotic phase, which occurs because cancer cells frequently have defective apoptotic mechanisms. It occurs when cancer cells' DNA is extensively damaged by radiation and attempts to divide during mitosis, resulting in incomplete cell division or cells with aberrant chromosomes that may die in the first or subsequent cycles of division.

    2.4. Autophagy is a dying process that relies on lysosome enzymes and is triggered by cellular stresses such as infection, toxin exposure, inadequate nutrition, and radiation. This sort of death has a process that produces an autophagosome, which connects with the lysosome to form an autolysosome and eventually decomposes (54-57).

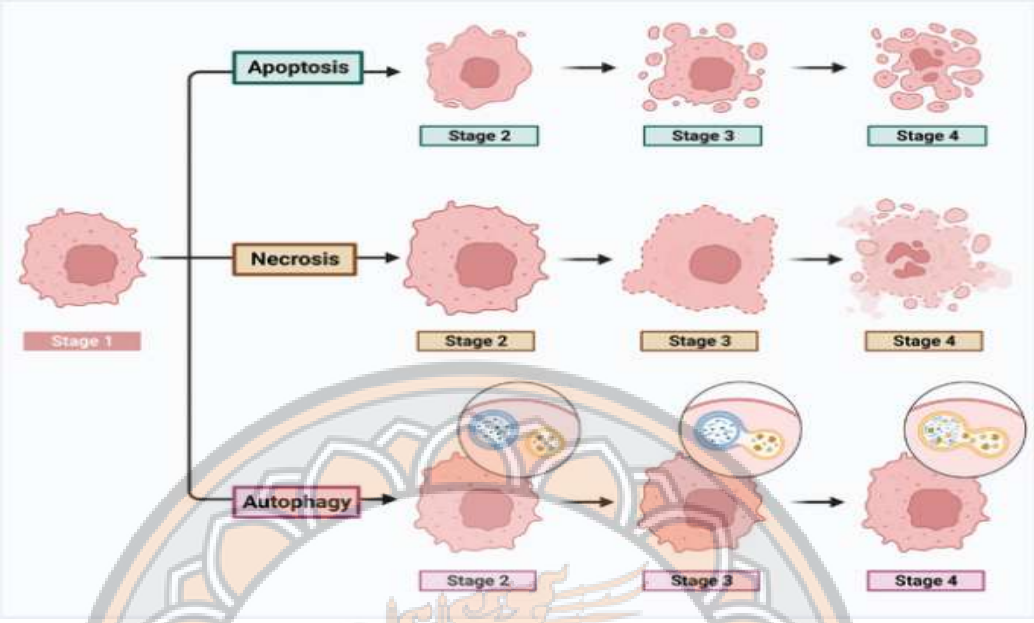

Figure 3 The basic processes of apoptosis, necrosis, and autophagy.

Source: Zhu X, Li S. Ferroptosis, Necroptosis, and Pyroptosis in Gastrointestinal Cancers: The Chief Culprits of Tumor Progression and Drug Resistance. Advanced Science. 2023;10.

2.4 Reactive Oxygen Species (ROS) in Radiation Biology

1. Radiation-induced ROS generation

Ionizing radiation mainly produces ROS through water radiolysis because water is the primary component of cells and absorbs much of the deposited energy. Water radiolysis quickly forms short-lived reactive intermediates that develop into biologically important ROS, leading to an early oxidative burst immediately after IR. The main ROS discussed in radiobiology include hydroxyl radicals (•OH), superoxide anions ($O_2^{\bullet -}$), and hydrogen peroxide (H_2O_2), which vary in reactivity, diffusion distance, and lifespan in aqueous environments. Among these, OH is generally viewed as the most reactive and damaging because it reacts close to where it forms and can attack DNA, proteins, and lipids on a near-diffusion-limited timescale. In mammalian systems, much radiation-induced damage occurs through indirect action, where ROS produced by water radiolysis cause chemical harm to vital biomolecules rather than radiation directly hitting DNA. Therefore, ROS-driven processes often dominate radiation-related DNA damage under oxygen-rich, watery cellular conditions, highlighting ROS as key molecular agents in the radiation response (58, 59).

2. ROS-mediated cellular damage

ROS can induce DNA damage, including base oxidation and strand breaks, by chemically modifying DNA components. In cancer cells, ROS also interact with the DNA damage response (DDR), where oxidative lesions can activate checkpoint signaling and influence repair pathway choices, affecting how cells handle or accumulate genomic damage (60). Beyond nuclear DNA, ROS are closely associated with mitochondrial dysfunction because mitochondria are both a major source of endogenous ROS and a vulnerable target of oxidative injury. Oxidative stress can damage mitochondrial lipids, proteins, and DNA, which may impair electron transport and lead to increased ROS production, creating a vicious cycle of mitochondrial damage and redox imbalance (61). The term oxidative stress is generally defined as a condition in which ROS production exceeds antioxidant defenses, resulting in damage to macromolecules and disrupted cell signaling. Therefore, ROS-mediated cellular damage is best viewed as an integrated process, where oxidative lesions compromise DNA integrity and mitochondrial function while simultaneously altering redox-regulated signaling networks (62).

3. ROS-mediated cell death pathways

ROS promote intrinsic (mitochondrial) apoptosis by causing mitochondrial damage, loss of mitochondrial membrane integrity, and activating downstream pro-apoptotic signals that lead to caspase activation. In radiobiological settings, excessive oxidative stress can push cells beyond adaptive responses and toward apoptosis, especially when mitochondrial damage is extensive or persistent (63). Radiation and oxidative injury can also result in mitotic catastrophe; a form of cell death linked to abnormal mitosis that often results from unrepaired DNA damage and disrupted progression through the G2/M boundary. Mitotic catastrophe is often described as occurring during or after faulty mitosis due to defective checkpoint control, connecting DNA damage to lethal errors in chromosome segregation (64). ROS also contribute to G2/M arrest because oxidative DNA lesions activate checkpoint signaling, which can pause the cell cycle to allow repair. However, prolonged arrest may increase the risk of cell death pathways (65). Because G2/M is generally considered a relatively radiosensitive phase, ROS-induced damage accumulation and checkpoint activation around G2/M can influence radiosensitivity by determining whether cells successfully repair or undergo lethal mitosis.

4. ROS and radiosensitization

A central concept in radiosensitization is that ROS overload can increase the magnitude and persistence of radiation-associated DNA lesions, thereby shifting damage from repairable to lethal states (66). Persistent DNA double-strand break signaling is commonly monitored using γ-H2AX foci, which serve as a widely used biomarker of DNA damage and repair kinetics in radiobiology and translational studies. Mechanistically, phosphorylation of H2AX is linked to recruitment and organization of DNA repair factors at damaged chromatin, making γ-H2AX dynamics informative about ongoing repair processes (67, 68). Radiosensitization strategies that impair DNA repair frequently correlate with

increased or prolonged γ-H2AX foci, consistent with the interpretation of unrepaired or slowly repaired DSBs (69).

Taken together, ROS-centered radiosensitization frameworks link oxidative amplification to DNA damage persistence, γ-H2AX retention, and functional inhibition pf repair, providing a mechanistic bridge between oxidative stress biology and improved RT efficacy.

2.5 Radiosensitizer

The primary goal of cancer treatment is to achieve effective local tumor control while preventing distant metastasis. Historically, the treatment of cancers such as cervical, brain, head and neck cancers using a single therapeutic modality often resulted in high rates of local recurrence, leading to suboptimal clinical outcomes. Consequently, mixed-modality treatment strategies, including surgery combined with RT and chemotherapy, were developed to enhance tumor control and improve patient survival (70-72).

Radiosensitizers are agents that enhance the cytotoxic effects of ionizing radiation on tumor cells while ideally limiting damage to surrounding normal tissues. The use of radiosensitizers aims to overcome intrinsic or acquired radioresistance and thereby improve the therapeutic efficacy of RT without increasing radiation dose. Mechanistically, radiosensitization can occur at different stages of radiation interaction with biological systems and is broadly classified into physical, chemical, and biological mechanisms (73, 74).

At the physical level, radiosensitization involves enhancement of local energy deposition following IR. Materials with high electron density or high atomic number can increase radiation absorption and secondary electron production, leading to amplified initial physical damage within tumor cells. Although physical radiosensitization is most prominent in nanoparticle-based approaches, it represents the earliest stage of radiation interaction that can influence subsequent chemical and biological responses (75, 76).

At the chemical level, radiosensitizers modulate the radiolysis of water induced by ionizing radiation and the subsequent generation of ROS. Because most of the radiation-induced DNA damage occurs through indirect action mediated by ROS, compounds that enhance ROS production or impair cellular antioxidant defenses can intensify oxidative damage to DNA, proteins, and cellular membranes. This chemical amplification of oxidative stress contributes to increased DSBs and enhances radiosensitivity (58, 77).

At the biological level, radiosensitizers influence cellular responses to radiation-induced damage by modulating DNA repair pathways, cell cycle progression, and cell death signaling. Inhibition or delay of DSBs repair prolongs DNA damage signaling and increases the likelihood of lethal chromosomal aberrations. Additionally, redistribution of tumor cells into radiosensitive phases of the cell cycle, particularly the G2/M phase, further enhances radiation-induced cytotoxicity and reduces long-term clonogenic survival, which is the principal determinant of tumor control following RT (78-80).

Based on these physical, chemical, and biological mechanisms, a wide range of radiosensitizers has been investigated and incorporated into experimental and clinical RT protocols. Many commonly used chemotherapeutic agents act predominantly through chemical and biological radiosensitization by enhancing DNA damage and impairing repair processes when combined with radiation. Representative examples include:

1. Cisplatin is a chemotherapeutic medication that increases radiation sensitivity. It operates by adhering to cancer cells' DNA, producing DNA crosslinking, and preventing the repair of radiation-damaged DNA. It is highly specific to cervical cancer and head and neck cancers (72, 81).
2. 5-Fluorouracil (5-FU) is a medication that reduces the production of DNA and RNA in cancer cells (82), providing them with less resistance to radiation damage. It is extremely effective in gastrointestinal cancers, especially colorectal cancer (83).
3. Temozolomide is a chemotherapeutic medication that can cross the blood-brain barrier. It operates by damaging cancer cells' DNA and boosting their sensitivity to radiation, especially in glioblastoma cells (84).

2.6 Natural compounds as radiosensitizers

Currently, various synthetic radiosensitizers with different mechanisms of action have been developed. However, their clinical applications are often limited due to toxicity concerns. Traditionally used in cancer prevention, natural compounds are now being evaluated as alternative radiosensitizers. These natural substances are particularly interesting because they offer multiple benefits: functioning as antioxidants, anticancer, enhancing the immune system function, having proven safety profiles, and acting as radiosensitizers while protecting normal tissues from radiation damage (Figure 4 and 5). This dual role-enhancing radiation's effectiveness against cancer cells while protecting normal tissue-makes these compounds increasingly valuable in treating several types of cancer (85). Such as

1. **Curcumin**, a polyphenol derived from Curcuma longa L., has demonstrated significant potential as a radiosensitizer across various cancer types. Research has shown that curcumin enhances radiation sensitivity through multiple mechanisms, including downregulation of antioxidant enzymes, increased ROS generation, modulation of gene expression (including MDR1 and microRNAs), inhibition of NF-kB signaling, and regulation of various cellular pathways. Its radiosensitizing effects have been demonstrated in numerous cancer types, including head and neck, cervical, nasopharyngeal, bladder, esophageal, hepatocellular, pancreatic, renal cell carcinoma, lymphoma, lung cancer, melanoma, prostate cancer, and glioblastoma. Recent advances have also explored the use of curcumin in nano formulations, particularly when combined with other natural compounds like naringenin, showing enhanced radiosensitization effects in breast cancer both in vitro and in vivo through magnetic field-responsive nanocarriers (86-89).

2. **Plumbagin**, a natural naphthoquinone compound extracted from the medicinal plant Plumbago zeylanica L, has demonstrated anticancer properties against various malignancies, including breast cancer, lung cancer, ovarian cancer, acute myeloid leukemia (AML), and prostate cancer, both in laboratory and animal studies. Research has shown its potential as a radiosensitizer in multiple cancers, particularly in cervical cancer and melanoma. PL enhances radiation sensitivity in cervical cancer C33A cells by increasing caspase-3 activation, Bcl-2, surviving expression, and promoting apoptotic cell death. In melanoma B16F1 cells, it works by inducing oxidative stress, Bax, cytochrome-c, p53, PARP expression, and DNA damage, with its radiosensitizing effects also confirmed in mouse melanoma cells (15, 90, 91).
3. **Resveratrol**, a natural phytoalexin predominantly found in grapes, peanuts, and berries, demonstrates multiple therapeutic properties, including anti-inflammatory, anti-oxidative, and anti-cancer effects. Research has shown its effectiveness as a radiosensitizer across various cancer types, including breast cancer (MCF 7), colon carcinoma (CT26), melanoma (B16F10), hypopharyngeal carcinoma (FADU), nasopharyngeal carcinoma (CNE-1), prostate cancer (PC-3, DU145), and glioblastoma stem cells (SU-2). Its radiosensitizing mechanisms include inducing apoptosis and necrosis/senescence, generating ROS, causing cell cycle arrest, inhibiting p-AKT, downregulating E2F1 transcription factor, increasing perforin and granzyme-B expression, decreasing CD133 expression, and inhibiting NF-kB. Notably, in combination with RT, Res has shown promising results in improving survival rates in experimental models (92-95).

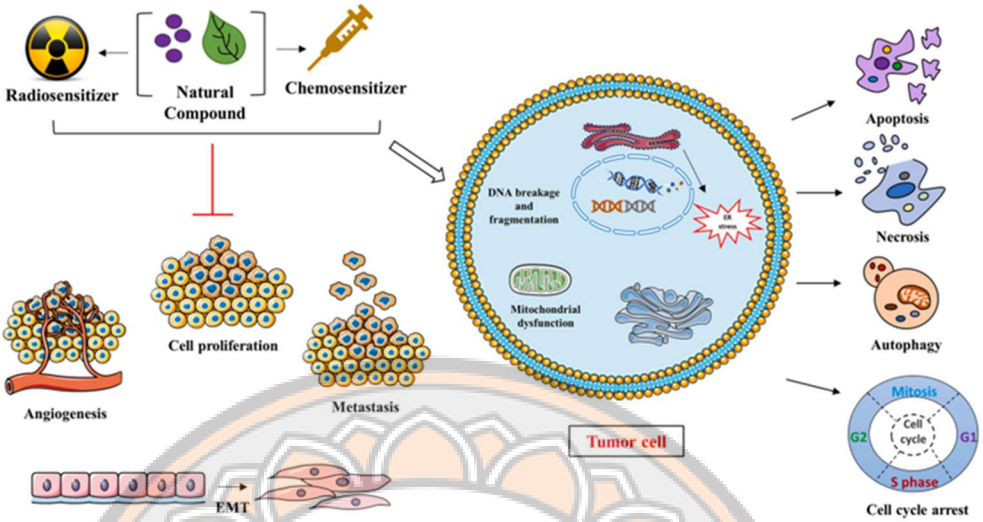

Figure 4 The mechanism of natural compounds as radio- and chemosensitizers.

Source: Nisar S, Masoodi T, Prabhu KS, Kuttikrishnan S, Zarif L, Khatoon S, et al. Natural products such as chemo-radiation therapy sensitizers in cancers. Biomedicine & Pharmacotherapy. 2022;154:113610.

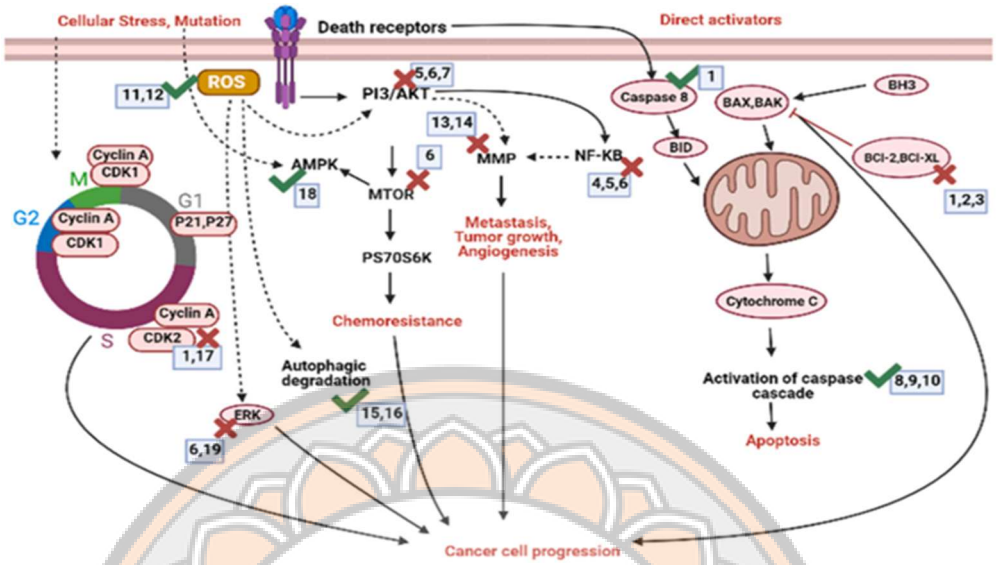

Figure 5 Signaling pathways affected by natural products in cancer cells; X indicates pathway inhibition, whereas √ indicates pathway activation of natural compounds via chemosensitizing/radiosensitizing effects. Numbers refer to natural compounds reported in the source article.

Source: Nisar S, Masoodi T, Prabhu KS, Kuttikrishnan S, Zarif L, Khatoon S, et al. Natural products as chemo-radiation therapy sensitizers in cancers. Biomedicine & Pharmacotherapy. 2022;154:113610.

2.7 Alpha-Mangostin (AM)

AM (*Garcinia Mangostana L.*) is a fruit that grows naturally in Southeast Asia and many other countries worldwide. AM is an extract derived from mangosteen peel containing most of the xanthone group (Figure 6). The yellow-green latex within the mangosteen peel's latex tube contains up to 78% of the total xanthone compound. It has been used as a folk remedy to heal various ailments, including infected wounds and other infections. AM has been shown in multiple studies to have anti-cancer, pain relief, antioxidant, antivirus and bacterial infections, anti-allergic, heart disease prevention, and neurological protection properties (96, 97). Because of these studies, it has been used to make many dietary supplements and cosmetics. It is also widely used in medicine due to its anti-inflammatory and antioxidant properties.

AM is gaining popularity in oncology since several studies have demonstrated its anti-cancer effects. As a result, there is research on the impact of alpha-mangosteen on several kinds of cancer cells, such as:

1. In breast cancer cells, When treated with AM at concentrations of 0, 1, 2, 3, 4, 6, 8, and 10 µM was given to MCF-7 breast cancer cells (IC50 = 3.57 µM) and MDA-

MB-231 (IC50 = 3.35 µM), the results of the study revealed that AM has a mechanism to inhibit the synthesis of intracellular fatty acid (FAS) via the action of FAK, ERK1/2, and AKT, causing the cells to undergo apoptosis (98).

2. In lung cancer cells. The study discovered that when AM at doses ranging from 0-100 µM was given to A549 lung cancer cells (IC50 = 19 µM) and CCD-14Br normal lung cells (IC50 = 22 µM), AM inhibited lung cancer metastasis (99).
3. In prostate cancer cells. The study found that when AM was given to LNCaP (IC50 = 5.9 µM), PC3 (IC50 = 12.7 µM), DU145 (IC50 = 22.5 µM), and 22Rv1 (IC50 = 6.9 µM) prostate cancer cells, the results demonstrated that AM has an effect in inhibiting the progression of the cell cycle. Through the activity of JNK and CDK proteins (100).
4. In cervical cancer cells, when AM was given to HeLa and SiHa at doses ranging from 20-30 µM (in vitro) and 20 and 40 mg/kg in mice by subcutaneous injection three times/week (in vivo). The study found that AM decreased mitochondrial membrane potential (MMP), resulting in the release of cytochrome C and increased levels of the apoptosis-inducing protein Bax, decreased levels of the apoptosis-preventing protein Bcl-2, and promoted the production of reactive oxygen species (ROS), which activated the p38 MAPK signaling pathway. Furthermore, mouse experiments showed that AM could reduce the size and weight of the tumors without affecting the overall health of the mice (101).

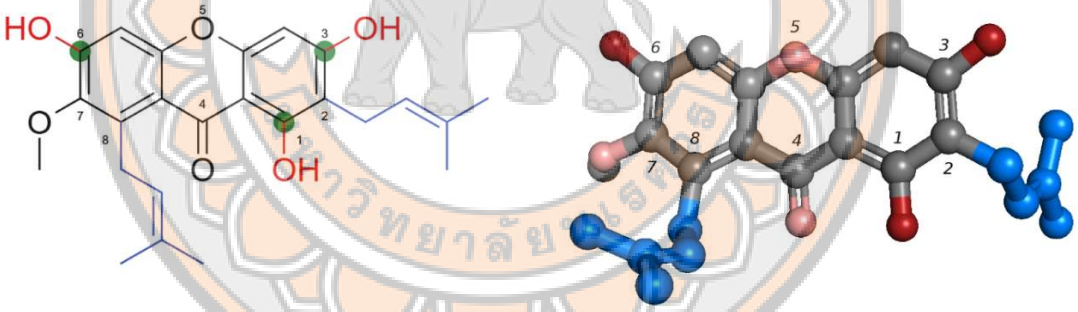

Figure 6 Comparison of 2D and 3D structures of AM with atom numbering according to IUPAC convention

Source: H. Górecka, M. Guźniczak, I. Buzalewicz, A. Ulatowska-Jarża, K. Korzekwa and A. Kaczorowska. International Journal of Molecular Sciences 2025 Vol. 26 Issue 11 Pages 5281. Accession Number: doi:10.3390/ijms26115281

CHAPTER III

RESEARCH METHODOLOGY

This research was conducted at the Faculty of Allied Health Sciences and Department of Radiology, Faculty of Medicine, Naresuan University

3.1 Materials and equipment.

The materials and equipment employed in this study are summarized in Table 1-3. Specially, Table 1 presents the cell lines used in the research, Table 2 lists the chemicals used in the experiments, and Table 3 summarizes the equipment used in the study.

Table 1 Cells used in the research.

Number	Cell	Abbreviation	Contributor
1	Human Cervical Cancer Cell Lines	HeLa	Assoc. Prof. Dr. Nipaporn Ngernyuang from Thammasat University, Thailand.
2	Human Fibroblast Cells Lines	CCD	Assoc. Prof. Dr. Kanchana Usuwanthim from Naresuan University, Thailand.

Table 2 Chemicals used in research.

Number	Chemicals	Abbreviation	Manufacturer
1	Alpha-Mangostin (Lot# 24375)	AM	MedChem Express LLC (MCE), USA
2	Dulbecco's Modified Eagle Medium	DMEM	Gibco, New York, USA
3	3-(4,5-dimethylthiazol-2-yl)-2,5-diphenyltetrazolium bromide	MTT	Thermo Fisher Scientific, China
4	Phosphate-buffered saline	PBS	Gibco, New York, USA
5	0.25% Trypsin EDTA	Trypsin	Gibco, New York, USA
6	Dimethyl Sulfoxide	DMSO	Loba Chemie, India
7	0.01% Crystal Violet	-	Loba Chemie, India
8	70% Ethanol	-	RCI Labscan, Bankok, Thailand
9	Muse® Cell Cycle Kit	-	Luminex, Texas, USA
10	Muse® Annexin V & Dead Cell Kit	-	Luminex, Texas, USA
11	4%Paraformaldehyde	-	Thermo Fisher Scientific, China
12	0.5% Triton X-100	-	
13	2% bovine serum albumin	BSA	Loba Chemie, India

Table 2 Chemicals used in research (continued).

Number	Chemicals	Abbreviation	Manufacturer
14	phosphohistone-H2AX (Ser139) monoclonal antibody (diluted 1:300),	-	Thermo Fisher Scientific, USA
15	Alexa-Fluor-488 conjugated polyclonal goat anti-mouse IgG antibody (diluted 1:500)	-	Gibco, New York, USA
16	4',6-diamidino-2-phenylindole	DAPI	Gibco, New York, USA
17	2'7'-dichlorofluorescin diacetate	H_2DCFDA	Invitrogen™ Molecular Probe, USA
18	Fetal Bovine Serum	FBS	Gibco, New York, USA
19	Penicillin Streptomycin	Pen Strep	Gibco, New York, USA
20	0.4% Trypan blue stain	-	Gibco, New York, USA
21	Slow Fade® Gold antifade reagent with DAPI	-	Invitrogen™ Molecular Probe, USA
22	Antibiotic-Antimycotic	Anti-Anti	Gibco, New York, USA

Table 3 Equipment used in research.

	Equipment	Manufacturer
1	Linear Accelerator, Clinac 2100 CD No. 5515	Varian
2	Bolus	Varian
3	Solid Phantom	Varian
4	Biosafety Cabinets	NuAire
5	CO_2 Incubator	SL SHEL LAB
6	Muse® Cell Analyzer	Luminex, Texas, USA
7	Microplate Reader	Molecular Devices, USA
8	Centrifuge	Hettich
9	Hemocytometer	HBG® BLOOD COUNTING CHAMBER BRIGHTLINE
10	Carl Zeiss fluorescence microscope	Carl Zeiss AG, Germany

3.2 Cell Culture and Cell Lines

HeLa cervical cancer cells and fibroblast cells were cultured in Dulbecco's Modified Eagle's Medium (DMEM) supplemented with 10% fetal bovine serum (FBS) and 1% penicillin/streptomycin and maintained at 37 °C in a humidified incubator with 95% air and 5% CO_2. The DMEM was changed every 3-4 days and once the cells reached 80% confluence, cells were sub-cultured with 0.25% trypsin.

3.3 Cytotoxicity Evaluation and Determine Inhibitory Concentration 20 (IC20)

A 3-(4,5 Dimethylthiazol-2-yl)-2,5-Diphenyltetrazolium bromide (MTT) assay was performed to assess the viability of HeLa cells after 24 hours of cell culture with varying concentrations of AM. The percentage of cell viability was measured to identify the concentrations of AM that caused a 20% decrease in the growth of HeLa cells (Inhibitory concentration; IC20), which will be used in further experiments (Figure 7).

1. HeLa cells were seeded into 96-well plates at density of $1x10^4$ cells per well in 100 µL of complete DMEM per well and incubated at 37 °C in a humidified incubator with 5% CO_2 for 24 hours to allow attachment.
2. After 24 hours, the culture DMEM was removed, the cells were washed with phosphate-buffered saline (PBS), and AM at concentrations of 0, 5, 10, 15, 20, 25, 30, and 35 µM was added in 100 µL per well to complete DMEM. The treated cells were incubated at 37°C with 5% CO_2 for 24 hours.
3. At the end of incubation, the treatment DMEM was removed, and the cells were washed with PBS. MTT solution (0.5 mg/mL) prepared in serum-free DMEM was added to each well (100 µL per well), and the plates were incubated for 3 hours in the dark.
4. After incubation, the MTT solution was removed and replaced with 100 µL of DMSO to dissolve the formazan crystals. The absorbance was measured at 570 nm using a microplate reader.
5. Cell viability (%) was calculated using the following equation (1).

$$\text{Cell Viability}(\%) = \frac{\text{Absorbance of Treated Cell}}{\text{Absorbance of Untreated control Cell}} \times 100 \qquad (1)$$

6. The dose-response curve generated from the MTT assay was fitted using nonlinear regression analysis, and the IC20 value was derived from the fitted model for subsequent experiments.

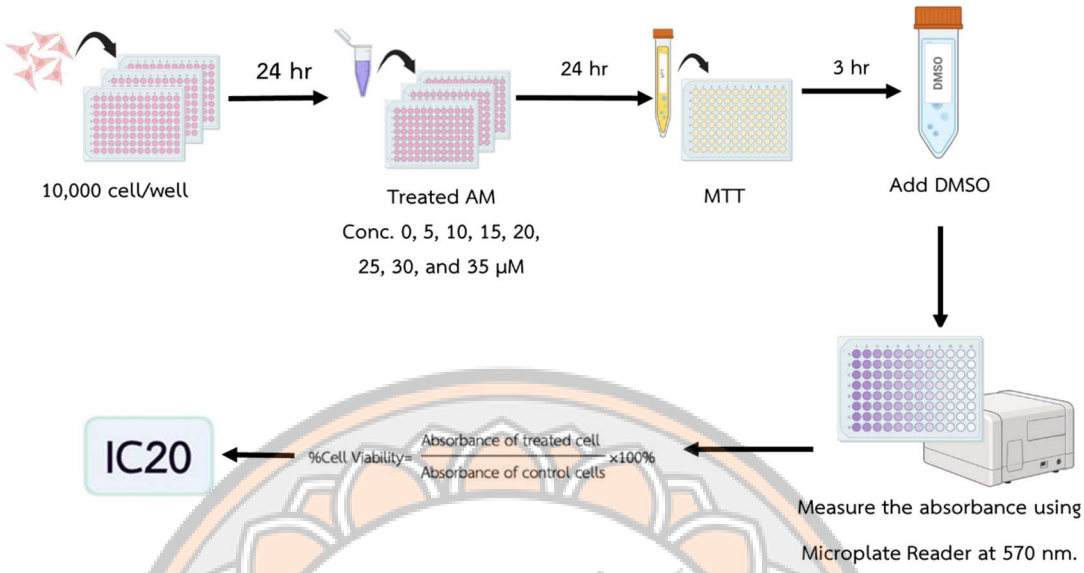

Figure 7 Schematic illustration of cytotoxicity of AM on HeLa cells (MTT assay).

3.4 Irradiation Setup

This experiment was conducted to establish a standardized IR condition for all radiation-related experiments in this study, including radiation-only and combination treatment experiments. The IR setup was designed to ensure dose uniformity at the cellular level and reproducibility across different experimental assays (Figure 8).

1. HeLa cells were seeded into 24-well plates at a density of $2x10^5$ cells per well in 2 mL of complete DMEM and incubated at 37 °C in a humidified incubator with 5% CO_2 for 24 hours to allow attachment.
2. For the combination experiment, the cells were pretreated with AM for 24 hours before IR.
3. Cell culture plates used for IR were prepared according to the experimental design and placed on a solid water phantom (30x30 cm^2 base, 15 cm thickness) to provide adequate backscatter during IR.
4. To achieve dose homogeneity within the cell monolayer, the plates were positioned between two 1.5 cm-thick tissue-equivalent bolus slabs, with an additional bolus slab placed on top of the plates.
5. IR was performed using a 6 MV linear accelerator under standardized IR geometry with a source-to-surface distance (SSD) of 96.5 cm and a field size of 15x20 cm^2.
6. The prescribed radiation dose was delivered in a single fraction as per the experimental protocol. Non-irradiated control groups were handled under identical conditions without radiation exposure.
7. Following IR, the cell culture DMEM was replaced with fresh complete DMEM, and the cells were returned to a 37°C incubator with 5% CO_2 for 24 hours for subsequent experimental procedures.

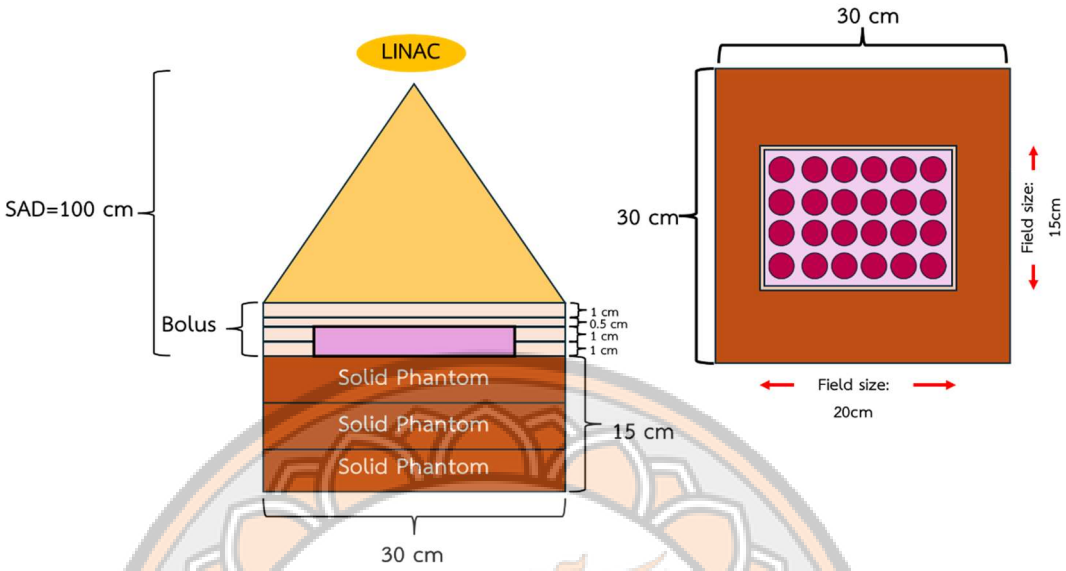

Figure 8 Schematic illustration of IR conditions for assessing radiosensitivity.

3.5 Radiation Lethal Dose 20 (LD20) Evaluation

To determine the lethal radiation dose for HeLa cells and establish a baseline radiation response for subsequent combination experiments, a clonogenic survival assay was performed. Cells were exposed to increasing single-fraction radiation doses, and long-term survival was assessed by colony-forming ability (Figure 9).

1. HeLa cells were seeded into 6-well plates at a density of $2x10^5$ cells per well in 2 mL of complete DMEM and incubated at 37 °C in a humidified incubator with 5% CO_2 for 24 hours to allow attachment.
2. The cells were irradiated at a single dose of 0, 1, 2, 4, and 6 Gy under the Irradiation Setup section (3.4).
3. After IR, the cells were replaced with DMEM and returned to a 37°C incubator with 5% CO_2 for an additional 24 hours.
4. After incubation, the culture DMEM was removed, and the cells were washed with PBS. The cells were detached using 0.25% Trypsin-EDTA for 3-5 minutes and neutralized with complete DMEM.
5. The cells were collected into a 15-mL Falcon tube and centrifuged at 1500 rpm for 5 minutes. The cell pellet was resuspended with 1 mL of complete DMEM.
6. The cells were counted using hemocytometry with trypan blue staining.
7. The cells were cultured in 6-well plates at densities ranging from 250 to 3,000 cells per well in 2 mL of DMEM, depending on the radiation dose.
8. The cells were incubated at 37°C in a 5% CO_2 incubator for 10 days without changing the culture DMEM.
9. After incubation, the culture DMEM was removed, and the cells were washed with PBS, fixed with methanol for 10 min, and stained with 0.5% crystal violet for 45 min. Excess stain was removed, and the plates were rinsed with distilled water and air-dried at room temperature.
10. Colonies containing more than 50 cells were counted under a light microscope. Plating efficiency (PE) and survival fraction (SF) were calculated using equation (2) and (3).
11. Radiation survival curves were generated by fitting the SF data to a linear–quadratic (LQ) model using GraphPad Prism version 10.5

$$PE=\frac{\text{No. of Colonies Formed}}{\text{No. of Cells Seeded}} \times 100 \quad (2)$$

$$SF=\frac{\text{No. of Colonies Formed After Treatment}}{\text{No. of Cells Seeded} \times PE} \times 100 \quad (3)$$

12. The LD20, defined as the radiation dose at which 80% cell survival was observed, was determined by interpolation of the radiation survival curve and was subsequently used in further combination experiments.

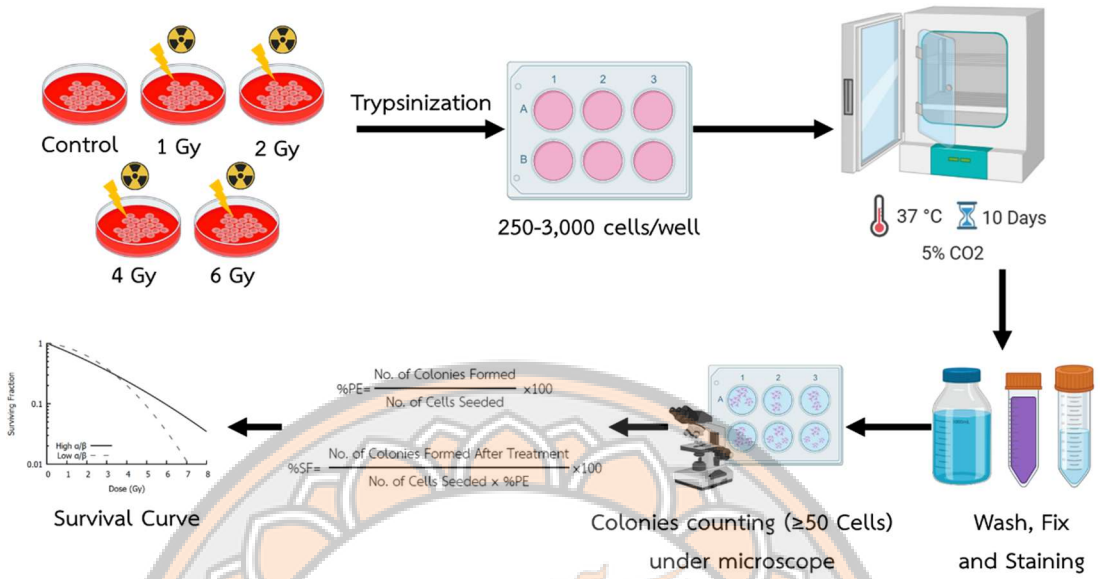

Figure 9 Schematic workflow of the clonogenic survival assay following radiation exposure.

3.6 Intracellular ROS detection by H_2DCFDA Assay

This experiment was performed to evaluate intracellular ROS generation in HeLa cells following treatment with AM, IR, or a combination of the two. Intracellular ROS levels were measured using the 2′,7′-dichlorofluorescein diacetate (H_2DCFDA) fluorescence assay, and ROS production in each treatment group was expressed relative to the untreated control group (Figure 10).

1. HeLa cells were seeded into 96-well plates at a density of 2×10^5 cells per well in 2 mL of complete DMEM and incubated at 37°C in a humidified incubator with 5% CO_2 overnight to allow cell attachment.
2. After incubation, the culture DMEM was removed, and the cells were incubated with 20 μM H_2DCFDA solution for 45 minutes at 37°C in the dark to allow intracellular loading of the probe.
3. Following H_2DCFDA incubation, the H_2DCFDA solution was removed, and 200 μL of fresh complete DMEM containing the designated treatment was added to each well.
4. Cells were treated according to the experimental design, including untreated control, AM treatment, IR treatment, and combination treatment (AM + IR). Cells in the AM and combination treatment groups were incubated with AM for 6 hours.
5. For IR groups, cells were irradiated under the photon IR conditions described in the Irradiation Setup section (3.4). Fluorescence intensity was measured at 2 hours after IR.
6. Fluorescence signals were measured using a fluorescence microplate reader at 485 nm excitation and 535 nm emission in end-point mode.
7. The fluorescence intensity obtained for each treatment group was normalized to the untreated control group, which was set to 1 to allow comparison of relative intracellular ROS levels across different experimental conditions.

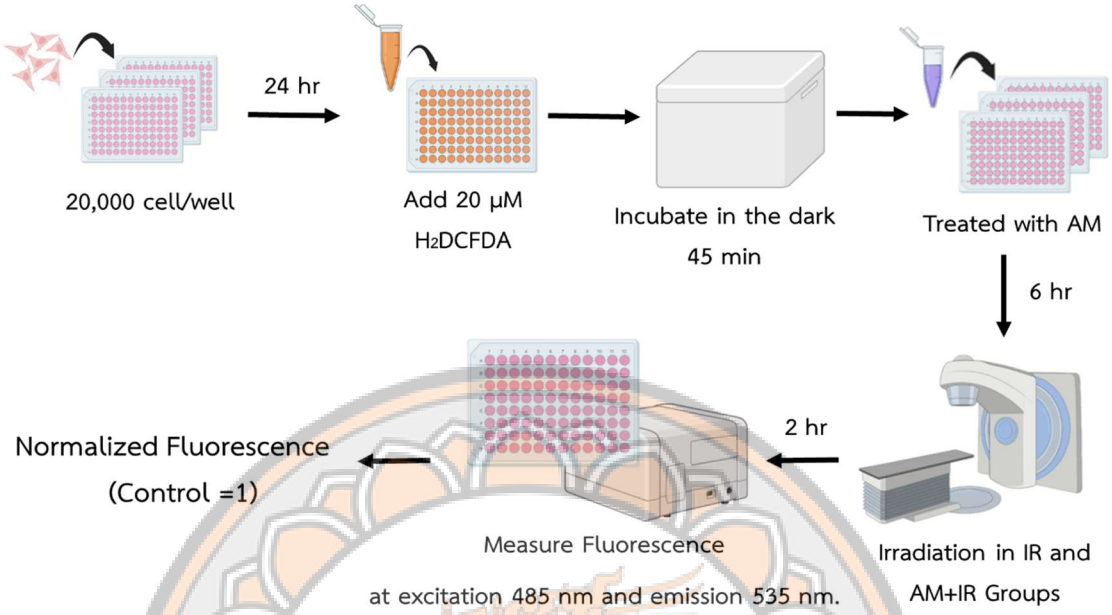

Figure 10 Schematic illustration of Intracellular ROS detection by H_2DCFDA Assay.

3.7 γ-H2AX Immunofluorescence Assay

This experiment was performed to evaluate DNA double-strand break (DSB) formation in HeLa cells following treatment with AM, IR, or a combination. DNA damage was assessed by immunofluorescence staining of phosphorylated histone H2AX (γ-H2AX), a well-established marker of radiation-induced DSBs (Figure 11).

1. HeLa cells were seeded onto sterile glass coverslips placed in 24-well plates at a density of $2x10^5$ cells per well in 2 mL of complete DMEM and incubated at 37 °C in a humidified incubator with 5% CO_2 for 24 hours to allow cell attachment.
2. Cells were treated according to the experimental design, including untreated control, AM treatment, IR treatment, and combination treatment (AM + IR). For AM and combination treatment groups, cells were pretreated with AM for 24 hours before IR.
3. Cells in the IR and combination treatment groups were exposed to photon IR under the conditions described in the Irradiation Setup section (3.4).
4. The culture DMEM was removed, and the cells were gently washed with PBS. Cells were then fixed with 4% paraformaldehyde for 15 minutes at room temperature, followed by PBS washes.
5. Fixed cells were permeabilized with 0.5% Triton X-100 in PBS for 10 minutes, washed with PBS, and subsequently blocked with 2% bovine serum albumin (BSA) in PBS for 1 hour at room temperature to reduce non-specific binding.
6. Cells were incubated with a primary antibody against γ-H2AX (Ser139) diluted in blocking solution and incubated overnight at 4 °C.
7. After primary antibody incubation, cells were washed with PBS and incubated with a fluorophore-conjugated secondary antibody for 1 hour at room temperature in the dark.
8. Cell nuclei were counterstained with 4′,6-diamidino-2-phenylindole (DAPI) for 5 minutes, followed by washing with PBS.
9. Coverslips were mounted onto glass slides using an antifade mounting medium. Fluorescent images were acquired using a fluorescence microscope under identical acquisition settings for all experimental groups.
10. Mean γ-H2AX fluorescence intensity per nucleus was quantified using ImageJ software version 1.53t. Nuclei were defined as regions of interest (ROIs) based on DAPI staining, and background-subtracted mean fluorescence intensity was measured for each nucleus.

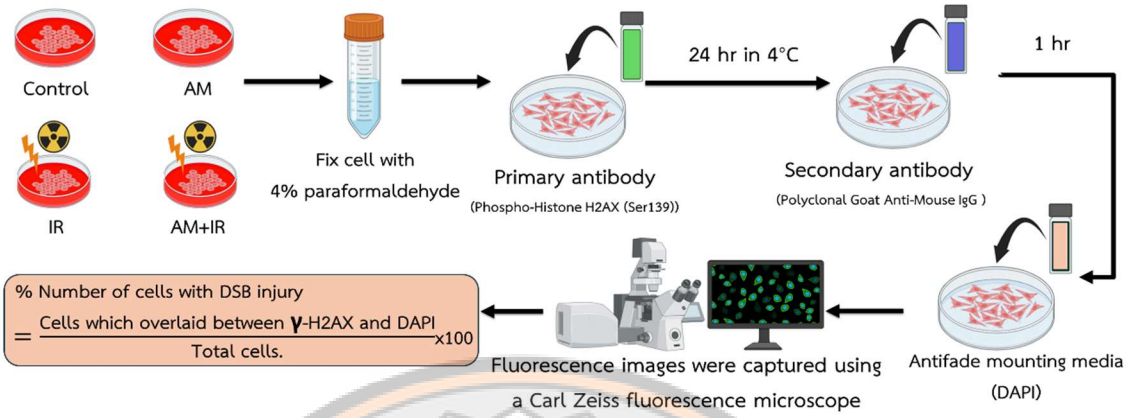

Figure 11 Schematic illustration of γ-H2AX Immunofluorescence Assay.

3.8 Cell cycle analysis

This experiment was performed to evaluate the effects of AM, IR, and combined treatment on cell cycle progression in HeLa cells, with the aim of determining whether treatment induces cell cycle arrest. Cell cycle distribution was analyzed by fluorescence-based DNA content assay (Figure 12).

1. HeLa cells were seeded into 24-well plates at a density of 2×10^5 cells per well in 2 mL of complete DMEM and incubated at 37°C in a humidified incubator with 5% CO_2 for 24 hours to allow cell attachment.
2. Cells were treated according to the experimental design, including untreated control, AM treatment, IR treatment, and combination treatment (AM + IR). For the AM and combination treatment groups, cells were pretreated with AM for 24 hours before IR.
3. For IR and combination treatment groups, cells were exposed to ionizing radiation under the conditions described in the Irradiation Setup section (3.4). Following IR, cells were further incubated for 24 hours at 37°C with 5% CO_2 and 95% relative humidity before cell cycle analysis.
4. The culture DMEM was removed, and cells were gently washed twice with 2 mL of PBS.
5. Cells were detached by adding 1 mL of 0.25% trypsin–EDTA to each well and incubating for 3–5 minutes at 37°C.
6. Trypsin activity was neutralized by adding 3 mL of fresh complete DMEM, and the cell suspension was collected into 15 mL Falcon tubes.
7. Cells were centrifuged at 1,500 rpm for 5 minutes to obtain a cell pellet.
8. The cell pellet was resuspended in 1 mL of DMEM, and cell numbers were determined using a hemocytometer with trypan blue staining.
9. Cells were adjusted to a density of 1×10^5 cells per 500 µL of culture DMEM and transferred into 1.5 mL microcentrifuge tubes.
10. Cell suspensions were centrifuged at 8,000 rpm for 7 minutes, and the supernatant was carefully removed.
11. Cell pellets were gently washed with 1 mL of PBS, taking care to avoid excessive mechanical disruption.
12. Cells were fixed by resuspension in 500 µL of cold 70% ethanol.
13. Fixed cells were stored at −20°C for at least 3 hours to preserve DNA integrity.
14. After fixation, 200 µL of the fixed cell suspension was transferred into new 1.5 mL microcentrifuge tubes.
15. The samples were centrifuged at 8,000 rpm for 7 minutes, and the ethanol was discarded.
16. Cell pellets were washed with 1 mL of PBS, then centrifuged at 8,000 rpm for 7 minutes; the PBS was removed.
17. 200 µL of Muse® Cell Cycle reagent was added to each tube, and cells were gently resuspended to obtain a single-cell suspension.

18. Samples were incubated in the dark at room temperature for 30 minutes, and cell cycle distribution was analyzed using a Muse® Cell Analyzer according to the manufacturer's instructions.

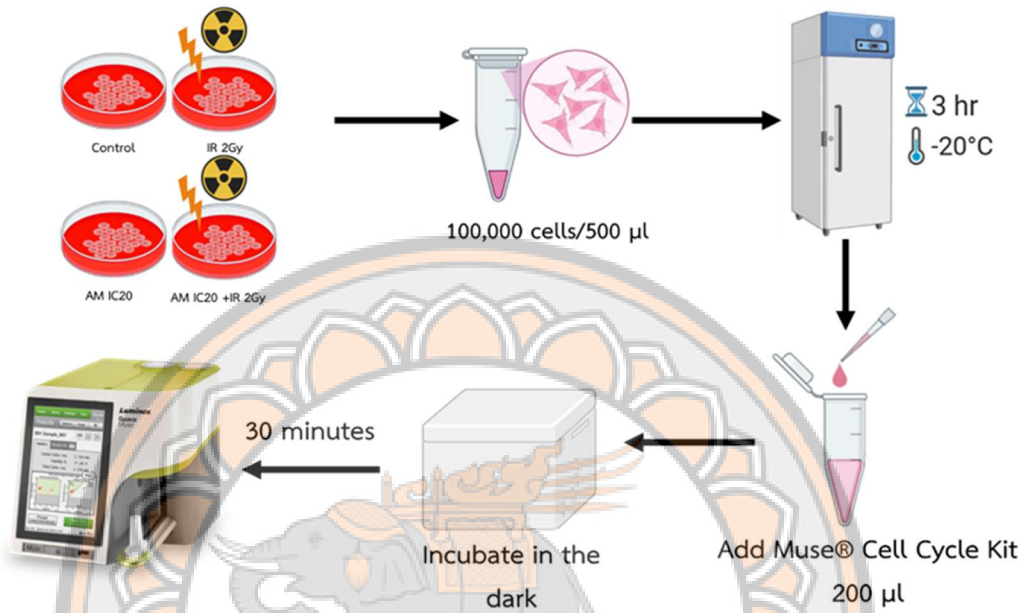

Figure 12 Schematic workflow of Cell cycle analysis.

3.9 Apoptosis Analysis

This experiment was performed to evaluate apoptotic cell death in HeLa cells following treatment with AM, IR, or a combination. Apoptosis was assessed using an Annexin V/propidium iodide (PI)-based staining method and analyzed using a Muse® Cell Analyzer according to the manufacturer's instructions (Figure 13).

1. HeLa cells were seeded into 24-well plates at a density of 2×10^5 cells per well in 2 mL of complete DMEM and incubated at 37°C in a humidified incubator with 5% CO_2 for 24 hours to allow cell attachment.
2. Cells were treated according to the experimental design, including untreated control, AM treatment, IR treatment, and combination treatment (AM + IR). For AM and combination treatment groups, cells were pretreated with AM for 24 hours before IR.
3. For IR and combination treatment groups, cells were exposed to IR under the conditions described in the Irradiation Setup section (3.4). Following IR, cells were incubated for an additional 24 hours at 37°C with 5% CO_2 prior to apoptosis analysis.
4. The culture DMEM was removed, and cells were gently washed with PBS.
5. Cells were detached using 0.25% trypsin–EDTA for 3–5 minutes, neutralized with complete DMEM, and collected into 15 mL Falcon tubes.
6. Cells were centrifuged at 1,500 rpm for 5 minutes to obtain a cell pellet.
7. The cell pellet was resuspended in 1 mL of DMEM, and cell numbers were determined using a hemocytometer with trypan blue staining.
8. Cells were adjusted to a density of 1×10^4 cells per sample in 100 µL of complete DMEM and transferred into 1.5 mL microcentrifuge tubes.
9. An equal volume (100 µL) of Muse® Annexin V & Dead Cell reagent was added to each sample, and the samples were incubated in the dark at room temperature for 30 minutes.
10. Samples were analyzed using a Muse® Cell Analyzer, and populations were reported as live, early apoptotic, late apoptotic, and dead/necrotic cells based on Annexin V and PI signals.

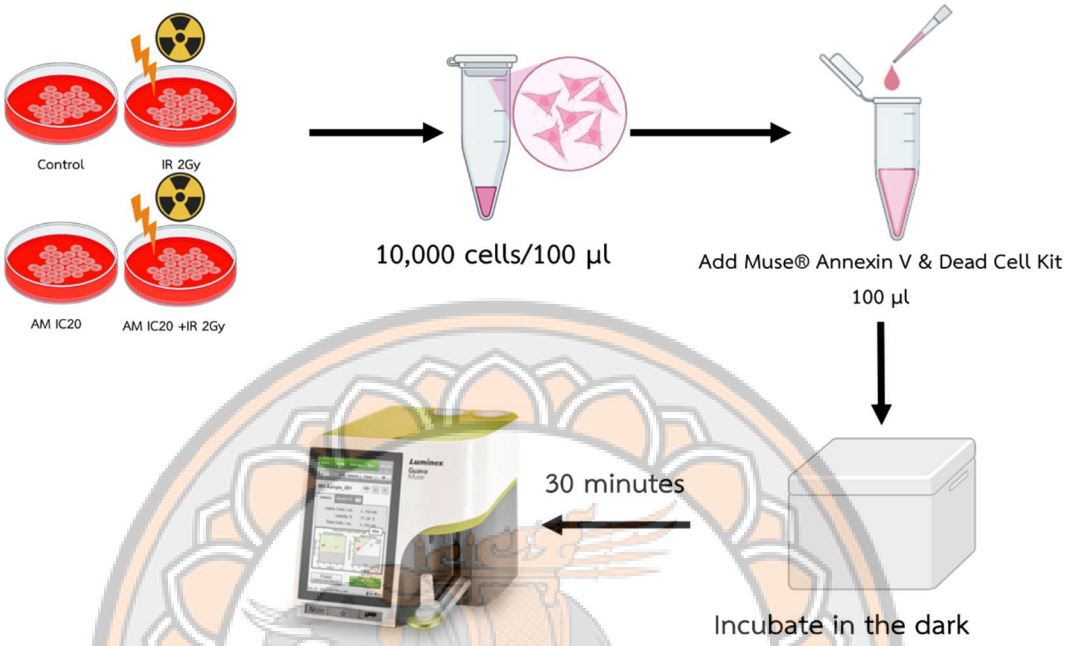

Figure 13 Schematic illustration of Apoptosis Analysis.

3.10 Clonogenic Assay

This experiment was performed to evaluate the long-term clonogenic survival of HeLa cells following treatment with AM, IR, or a combination. The clonogenic assay assesses the ability of a single cell to undergo unlimited division and form a colony and is considered the gold standard for evaluating cellular radiosensitivity (Figure 14).

1. HeLa cells were seeded into 24-well plates at a density of 2×10^5 cells per well in 2 mL of complete DMEM and incubated at 37°C in a humidified incubator with 5% CO_2 for 24 hours to allow cell attachment.
2. Cells were treated according to the experimental design, including untreated control, AM treatment, IR treatment, and combination treatment (AM + IR). For AM and combination treatment groups, cells were pretreated with AM for 24 hours before IR.
3. For IR and combination treatment groups, cells were exposed to IR under the conditions described in the Irradiation Setup section (3.4). Following IR, cells were incubated for an additional 24 hours at 37°C with 5% CO_2 prior to the clonogenic assay.
4. The culture DMEM was removed, and cells were gently washed with PBS.
5. Cells were detached using 0.25% trypsin–EDTA for 3–5 minutes, neutralized with complete DMEM, and collected into 15 mL Falcon tubes.
6. Cells were centrifuged at 1,500 rpm for 5 minutes to obtain a cell pellet.
7. The cell pellet was resuspended in 1 mL of DMEM, and cell numbers were determined using a hemocytometer with trypan blue staining.
8. Cells were re-seeded into 6-well plates in 2 mL of complete DMEM. For the untreated control group, cells were seeded at a density of 150 cells per well, whereas the treatment groups, including AM, IR, and combination treatment, were seeded at a density of 300 cells per well to ensure reliable colony formation.
9. The plates were incubated at 37 °C in a humidified incubator with 5% CO_2 for 10 days without changing the culture DMEM to allow colony formation.
10. After the incubation period, the culture DMEM was removed, and the colonies were gently washed with PBS.
11. Colonies were fixed with methanol for 10 minutes at room temperature and subsequently stained with 0.5% crystal violet for 45 minutes.
12. Excess stains were removed, and the plates were rinsed with distilled water and air-dried at room temperature.
13. Colonies containing more than 50 cells were counted manually under a light microscope.
14. Plating efficiency (PE) and surviving fraction (SF) were calculated using equation (2) and (3).

$$PE=\frac{\text{No. of Colonies Formed}}{\text{No. of Cells Seeded}}\times 100 \quad (2)$$

$$SF=\frac{\text{No. of Colonies Formed After Treatment}}{\text{No. of Cells Seeded}\times PE}\times 100 \quad (3)$$

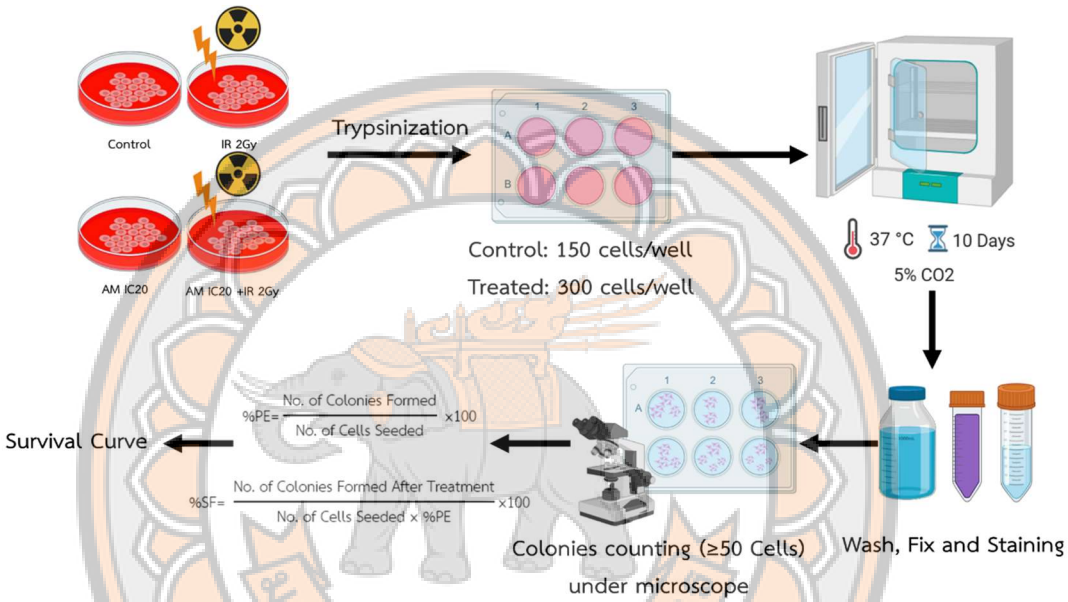

Figure 14 Schematic illustration of Clonogenic Assay.

3.11 Calculation of Sensitizer Enhancement Ratio (SER)

To quantitatively evaluate the radiosensitizing effect of AM in combination with IR, the SER was calculated based on clonogenic survival data.

The Sensitizer Enhancement Ratio (SER) was calculated to determine the ability of AM to enhance radiation-induced cell killing. This definition reflects the enhancement of radiation effectiveness required to achieve the same level of cell survival. In this study, SER was calculated using the equation (4)

$$SER = \frac{D_{IR\ alone}}{D_{AM+IR}} \text{ (at the same survival fraction; SF)} \quad (4)$$

where $D_{IR\ alone}$ represents the radiation dose required to achieve given SF in cells treated with IR alone, and D_{AM+IR} represents the radiation dose required to achieve the same SF in cells treated with AM in combination with IR. In this study, SER was estimated at a clinically relevant radiation dose of 2 Gy by comparing the SF between treatment groups. An SER value greater than 1 indicates a radiosensitizing effect, whereas an SER value equal to 1 indicates no enhancement of radiation response.

3.12 Statistical analysis

All experiments were performed in at least three independent experiments. Data are presented as mean ± standard deviation (SD). Statistical analyses were performed using GraphPad Prism version 10.5

For comparisons between two groups, an unpaired Student's T-test was used. For comparisons among three or more groups, one-way analysis of variance (one-way ANOVA) followed by Tukey's multiple comparisons test was applied. A p-value < 0.05 was considered statistically significant.

CHAPTER IV

RESULTS

4.1 Cytotoxicity Assessment and Determination of IC20 and LD20 Values of Alpha-Mangostin and Radiation in HeLa Cells.

MTT assays were performed to evaluate the cytotoxic effect of AM in HeLa cells and normal fibroblasts (after 24 hours of treatment with increasing concentrations of AM (0-35 µM; Figure 15A,B). In HeLa cells, AM treatment resulted in a concentration-dependent decrease in cell viability, with viability gradually declining from approximately 98% at 5 µM to 6.38% at 35 µM. Based on the dose-response relationship, the IC20 value of AM was estimated by interpolation to be approximately 13.67 µM (Figure 15A). The fitted equation used for IC20 estimation is shown in equation (5).

$$y = \frac{100}{\left(\frac{19.41}{x}\right)^{-3.957}+1}. \quad (5)$$

This concentration was considered appropriate for use as a sub-toxic dose in subsequent combination experiments.

In contrast, normal fibroblast exhibited greater tolerance to AM treatment, maintaining cell viability above 85% at concentrations up to 25 µM, with a marked reduction in viability observed only at concentrations greater than 30 µM (Figure 15B). These findings suggest a selective cytotoxic effect of AM on cervical cancer cells compared with normal fibroblasts and support selecting low AM concentrations for combination with radiation.

The radiation response of HeLa cells was subsequently assessed using a clonogenic survival assay following exposure to single radiation doses of 0, 1, 2, 4, and 6 Gy (Figure 15C). Clonogenic survival decreased progressively with increasing radiation dose, with the SF of 0.96, 0.66, 0.35, and 0.23 observed at 1, 2, 4, and 6 Gy, respectively. The survival data were fitted using LQ model, as shown in equation (6).

$$SF=e^{-(0.1191D+0.02791D^2)}. \quad (6)$$

From the dose-survival relationship, the lethal dose causing approximately 20% cell death (LD20) was estimated to be around 1.4 Gy.

Although the estimated LD20 was approximately 1.4 Gy, a radiation dose of 2 Gy, corresponding to approximately LD30 and representing the conventional clinical fractionated dose, was selected for subsequent experiments. Therefore, to avoid excessive baseline cytotoxicity associated with this higher radiation dose, the AM concentration used in combination experiments was slightly reduced from the calculated IC20 value (13.67 μM) to 12 μM (IC14).

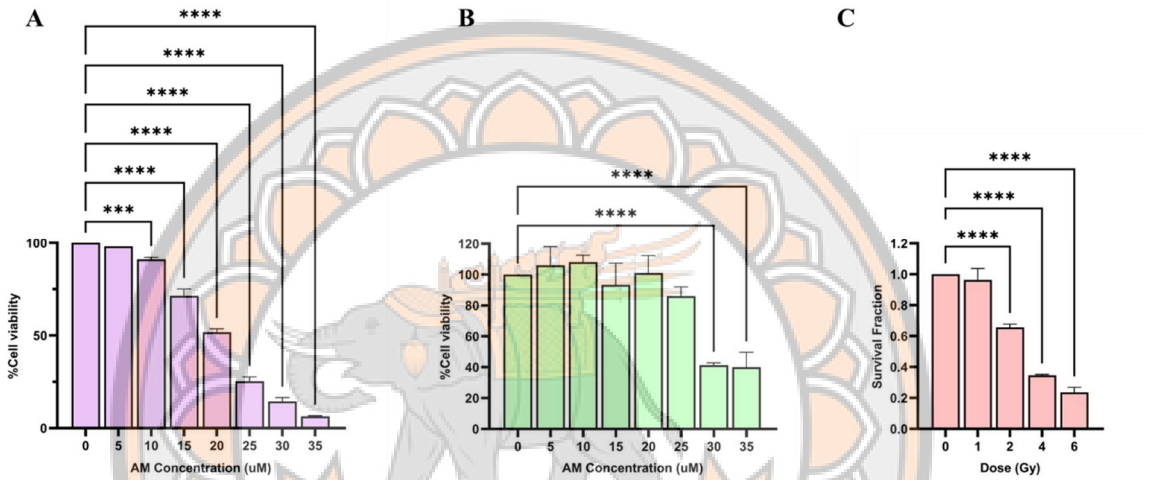

Figure 15 Determination of IC20 of AM and LD20 of radiation in HeLa cells. (A) Cytotoxicity of AM in HeLa cells after 24 hours treatment with increasing concentrations (0–35 μM), as determined by the MTT assay. (B) Cytotoxicity of AM in normal human fibroblasts under the same conditions. (C) Clonogenic survival of HeLa cells following exposure to single doses of ionizing radiation (0–6 Gy) for 10 days. Data are presented as mean ± SD from three independent experiments. Statistical significance: *** $p < 0.001$, **** $p < 0.0001$.

4.2 Effects of Alpha-Mangostin and Ionizing Radiation on Intercellular ROS Levels in HeLa Cells.

Intercellular ROS levels in HeLa cells were assessed by H_2DCFDA fluorescence staining and expressed as relative fluorescence intensity normalized to the control group, which exhibited baseline ROS levels and was set to 1.00.

The AM treatment group showed a slight increase in ROS levels (1.13 ± 0.05-fold relative to control); however, this change was not statistically significant, indicating that AM at the selected sub-toxic concentration did not induce substantial oxidative stress on its own.

In contrast, in the IR treatment group, ROS levels increased significantly to 3.32 ± 0.15-fold compared with control ($p<0.0001$). Notably, combination treatment led to a further significant elevation of ROS levels to 4.07 ± 0.18-fold compared with control ($p<0.0001$), which was also higher than with AM or IR alone, indicating that AM potentiated radiation-induced oxidative stress (Figure 16).

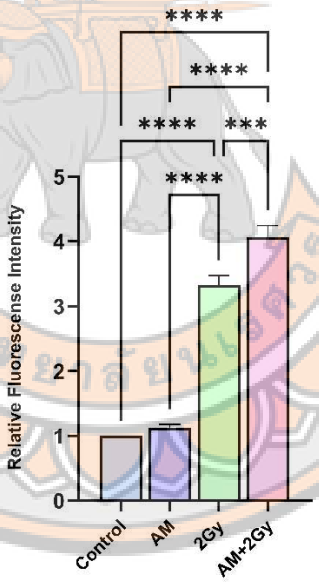

Figure 16 Effects of Alpha-Mangostin and ionizing radiation on intercellular ROS levels in HeLa Cells. Intercellular ROS levels in HeLa cells following treatment with AM, IR, and their combination, as determined by H_2DCFDA staining. Data are expressed as relative fluorescence intensity normalized to the control. Statistical significance: *** $p < 0.001$, ****$p < 0.0001$.

4.3 Alpha-Mangostin Induced DNA Damage Response Assessed by γ-H2AX Staining.

To investigate whether AM potentiates radiation-induced DNA damage, HeLa cells were evaluated by γ-H2AX immunofluorescence staining, and results were expressed as the percentage of γ-H2AX fluorescence intensity normalized to DAPI fluorescence within nucleus, calculated from the mean fluorescence intensities obtained from randomly selected fields of view as shown in Figure 17A.

Quantitative analysis revealed that in the AM treatment group, γ-H2AX intensity increased modestly but significantly to 12.26 ± 1.59% compared with the control group. In contrast, exposure to IR at 2 Gy resulted in a marked elevation of γ-H2AX expression to 25.94 ± 1.56%. Notably, combination treatment with AM and IR led to a pronounced increase in γ-H2AX intensity to 48.20 ± 6.60%, which was considerably higher than that observed with AM or IR alone. Furthermore, this increase represented approximately a two-fold enhancement relative to IR alone.

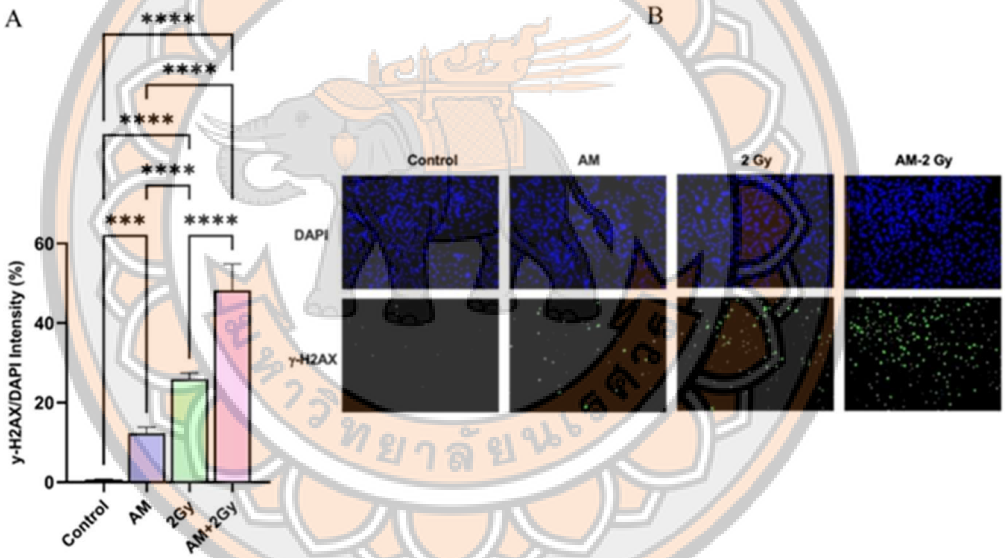

Figure 17 Effect of AM on radiation-induced DSBs in HeLa cells. (A) Quantification of γ-H2AX fluorescence intensity following treatment with AM, IR, and their combination. (B) Representative immunofluorescence images showing γ-H2AX positive signal (green) and DAPI-stained nuclei (blue) for each treatment condition. Statistical significance: *** $p < 0.001$, **** $p < 0.0001$.

Representative immunofluorescence images shown in Figure 17B were consistent with the quantitative analysis, showing minimal γ-H2AX signal in the control group and increase following AM, IR and especially the combination treatment group. Collectively, these results indicate that AM significantly potentiates radiation-induced DSBs and impairs their repair, consistent with its proposed role as a radiosensitizer.

4.4 Effects of Alpha-Mangostin and Ionizing Radiation on Cell Cycle Distribution in HeLa Cells

To investigate whether AM modulates cell cycle progression and contributes to radiosensitization, cell cycle distribution in HeLa cells was analyzed by flow cytometry following treatment with AM, IR, or the combination. Cell populations were quantified in the G0/G1, S, and G2/M phases based on DNA content, as shown in Figure 18A.

In the control group, most cells were in the G0/G1 phase (71.22%), with smaller proportions in the S (13.86%) and G2/M (14.18%) phases. Treatment with either AM or IR alone resulted in a significant reduction in the G0/G1 population compared with the control group (60.76% and 59.62%, respectively; $p < 0.001$). Correspondingly, both treatments led to an increase in the proportion of cells in the G2/M phase, indicating induction of cell cycle arrest at this checkpoint.

Notably, in combination treatment resulted in the most pronounced effect, elevating the G2/M fraction to 26.66% compared with 14.18% in control cells ($p < 0.001$). In contrast, no significant differences were observed among treatment groups in the S-phase population. Collectively, these results demonstrate that AM induces G2/M phase arrest in HeLa cells and enhances radiation-induced accumulation in this radiosensitive phase. This mechanistic effect suggests that AM potentiates radiosensitivity by delaying cell cycle progression at the G2/M checkpoint, thereby preventing DNA repair prior to mitotic entry.

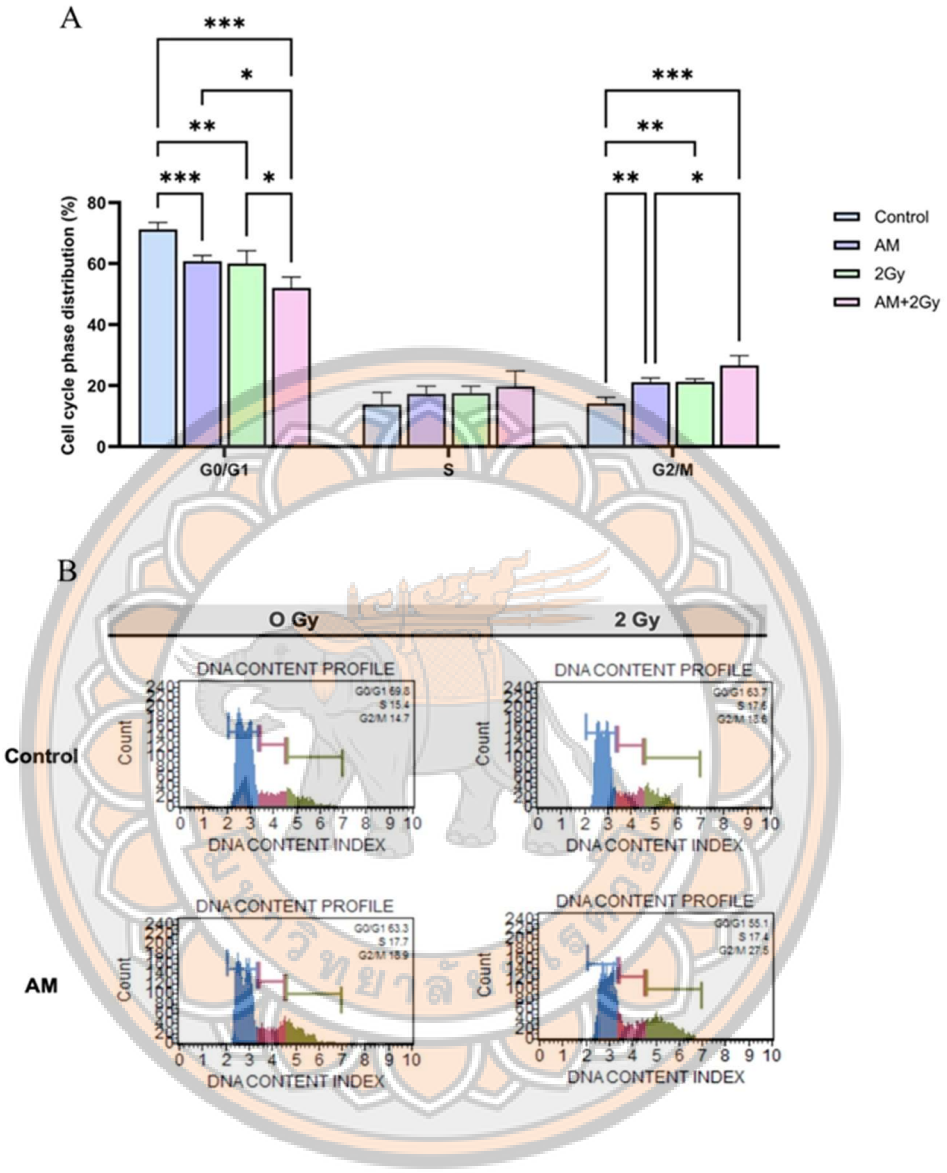

Figure 18 Effects of AM and IR on cell cycle distribution in HeLa cells. (A) Quantitative analysis of cell cycle phase distribution following treatments: control, AM, IR, and combination treatment. (B) Representative flow cytometry histograms of DNA content profiles. Cells were exposed to 0 Gy or 2 Gy radiation with/without AM pretreatment. Statistical significance: * $p < 0.05$, ** $p < 0.01$, *** $p < 0.001$.

4.5 Combined Alpha-Mangostin and Radiation Treatment Enhances Apoptosis in HeLa Cells.

To determine whether AM enhances radiation-induced cell death, apoptotic responses in HeLa cells were evaluated using Annexin V/PI staining followed by flow cytometric analysis (Figure 19). The proportions of apoptotic cells, including early and late apoptosis, were quantified to assess treatment-induced apoptotic effects.

As shown in Figure 19A, treatment with AM alone significantly increased the apoptotic population to 21.88% compared with 4.02% in the control group ($p < 0.001$). Treatment with IR alone resulted in a modest but significant increase in apoptosis (7.16%, $p < 0.01$ vs. control). Notably, in combination treatment group produced a pronounced elevation in apoptosis, reaching 39.48%, which was significantly higher than that observed with either AM or IR alone ($p < 0.0001$).

Representative flow cytometry dot plots (Figure 19B) supported these quantitative findings, demonstrating a marked increase in both early and late apoptotic cell populations in the combination treatment group compared with single-treatment conditions. These results indicate that AM markedly enhances radiation-induced apoptosis in HeLa cells, supporting its role as a potential radiosensitizer.

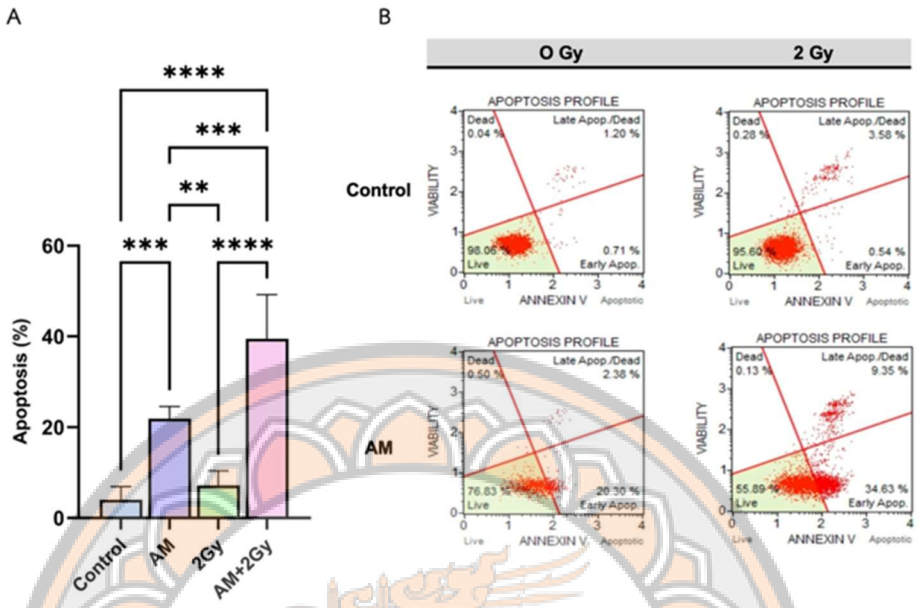

Figure 19 Combined AM and IR treatment enhances apoptosis in HeLa cells. (A) Quantification of apoptotic cells (% cell appearance) measured by Annexin V/Dead Cell assay 24 h after treatment with control, AM, IR, or the combination treatment. (B) Representative dot plots showing Annexin V and viability staining profiles for each treatment condition, with live cells (lower left quadrant), early apoptotic cells (lower right), late apoptotic/dead cells (upper right), and necrotic cells (upper left). Statistical significance: ** $p < 0.01$, *** $p < 0.001$,** $p < 0.0001$.**

4.6 Radiosensitizing Effect of Alpha-Mangostin Assessed by Clonogenic Survival Assay and Sensitizer Enhancement Ratio (SER)

The clonogenic assay was performed to evaluate the radiosensitizing effect of AM in HeLa cells following photon IR (Figure 20). Treatment with AM (12 μM) alone resulted in slightly a modest but significant reduction in clonogenic survival, with colony formation decreased to approximately 79% relative to the control group ($p < 0.01$). Furthermore, the IR group, which irradiated cells at 2 Gy alone further reduced cell survival to 62% of control levels ($p < 0.05$ vs. control).

Notably, combined treatment with AM and 2 Gy IR resulted in pronounced suppression of clonogenic survival, with only 28% of colonies remaining compared with the control group ($p < 0.0001$ vs. IR alone). Representative colony formation images (Figure 20B) corroborated these quantitative findings, showing markedly fewer and smaller colonies in the combination treatment group compared with either AM or radiation alone.

To quantitatively evaluate the radiosensitizing effect of AM, clonogenic survival data were further analyzed by calculating the sensitizer enhancement ratio (SER) at the same SF. The SER was defined as the ratio of radiation dose required to achieve the same SF in the absence and presence of AM.

In this study, the SF of the AM combined with IR at 2 Gy was 28% (SF= 0.28). Therefore, the radiation dose required to achieve the same SF in IR group was determined from fitting the SF data to a linear–quadratic (LQ) model and was estimated to be 4.95 Gy. The SER was calculated as follows:

$$SER = \frac{D_{\text{IR alone at SF 0.28}}}{D_{\text{AM+I at SF 0.28}}} = \frac{4.95}{2.00} \approx 2.48$$

This result indicates that the presence of AM substantially enhanced radiation-induced clonogenic cell killing. An SER value greater than 1 reflects a radiosensitizing effect, and the observed value suggests that AM exerts a strong radiosensitizing efficacy in HeLa cells.

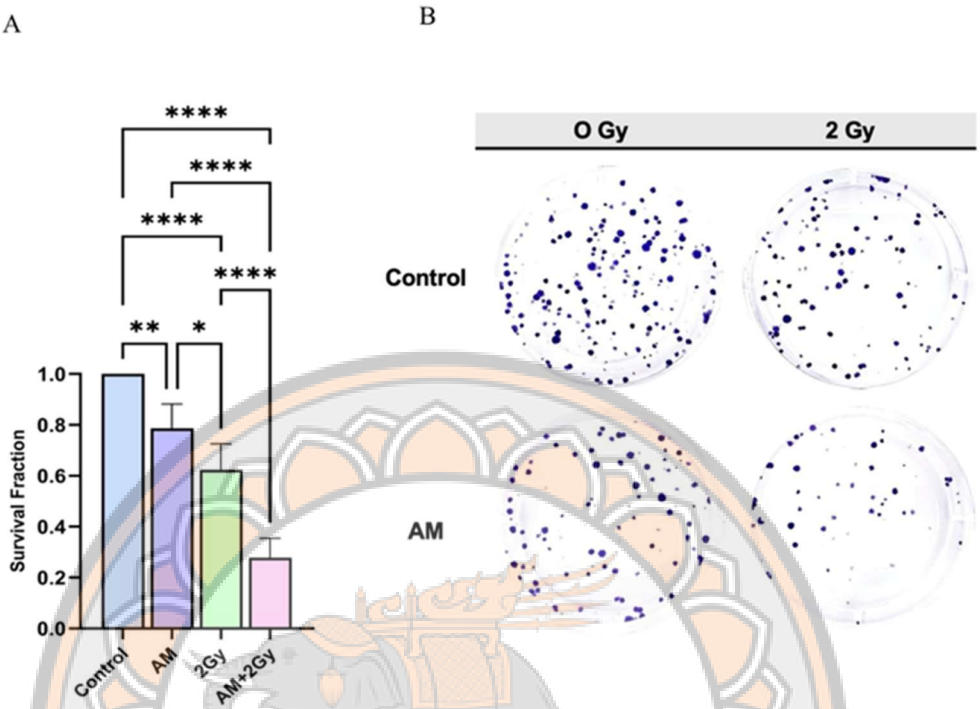

Figure 20 Radiosensitizing Effect of Alpha-Mangostin assessed by clonogenic survival assay. (A) Quantification of clonogenic SF in HeLa cells treated with control, AM, IR, or the combination treatment. (B) Representative images of crystal violet–stained colonies formed after 10 days under each treatment condition. Statistical significance: * $p < 0.05$, ** $p < 0.01$, **** $p < 0.0001$.

CHAPTER V

DISSCUSION

Alpha-Mangostin, a prenylated xanthone isolated from the pericarp of *Garcinia mangostana* has been widely reported to exhibit anticancer activity through mechanisms involving mitochondrial dysfunction, ROS generation, and apoptosis induction (102, 103). However, its potential role as a radiosensitizer has not been previously investigated. In the present study, AM exhibited dose-dependent cytotoxicity against HeLa cervical cancer cells (IC20 = 13.67 μM) while sparing normal fibroblasts (>85% viability at concentrations up to 25 μM) (Figure 14), indicating selective cytotoxicity at low concentrations (24, 104).

Radiosensitizers enhance tumor cell sensitivity to ionizing radiation through multiple mechanisms, including increased DNA damage, inhibition of DNA repair, modulation of cell cycle progression, and alleviation of tumor hypoxia, thereby enabling effective tumor control at lower radiation doses while minimizing injury to surrounding normal tissues (105, 106). To our knowledge, the present study is the first to demonstrate that AM enhances the radiosensitivity of HeLa cervical cancer cells to X-ray IR in vitro.

To reflect clinically relevant fractionated RT and to preserve sufficient post-IR survival for clonogenic analysis, AM at 12 μM (corresponding to IC_{14}) was combined with a single 2 Gy radiation dose (approximately LD_{30}), rather than using the conventional IC_{20}–LD_{20} combinations. This optimization prevented excessive baseline cytotoxicity, which could have obscured whether the observed effects were additive or synergistic, thereby allowing a more accurate evaluation of radiosensitization. Unlike cytotoxicity-based assessments, radiosensitization studies critically depend on post-IR survival as the primary endpoint, making lower, sub-lethal drug and radiation doses more appropriate for mechanistic interpretation.

In radiobiology, ionizing radiation induces cellular damage predominantly via indirect action, in which ROS generated from water radiolysis account for most of the radiation-induced DNA damage under normoxic conditions (107). In the present study, IR alone significantly increased intracellular ROS levels, induced DNA damage as indicated by γ-H2AX expression, promoted G2/M phase arrest, and reduced clonogenic survival (Figure 16, 17, 18, 20). Importantly, when AM was combined with ionizing radiation, intracellular ROS levels were further markedly elevated compared with radiation alone. This synergistic increase suggests that AM amplifies radiation-induced oxidative stress, potentially by disrupting cellular redox homeostasis or impairing antioxidant defense mechanisms, a phenomenon previously described for several natural radiosensitizers (108). Excessive ROS accumulation is known to promote DSBs formation and interfere with DNA repair processes, thereby enhancing radiosensitivity (105, 109).

Consistent with enhanced oxidative stress, γ-H2AX immunofluorescence analysis revealed that combination treatment markedly increased DNA damage compared with radiation alone (Figure 17), indicating enhanced DSB formation. γ-H2AX is a well-established surrogate marker of radiation-induced DSBs and activation of the DNA damage response (110, 111). Notably, the approximately two-fold increase in γ-H2AX signal observed following combination treatment at 1 hour post-IR suggests persistence of unrepaired DNA damage, a time point at which the majority of DSB repair is typically completed (112). Due to the combination treatment producing dense, overlapping γ-H2AX foci, signal intensity was used as a quantitative readout, providing a more reliable indicator of accumulated DSBs under these conditions (112, 113). Assessment of DNA damage at 1 hour post-IR reflects early DSB repair kinetics (114), whereas downstream cellular response, including cell cycle distribution, and apoptosis analysis, were evaluated at 24 hours post-IR to capture cell fate decisions following persistent DNA damage rather than immediate radiation injury (115, 116)

Following persistent DNA damage, cell cycle checkpoint activation is a critical downstream response that determines cell fate. Cells in the G2/M phase are recognized as the most radiosensitive due to chromatin condensation and limited DNA repair capability (117). In this study, both AM and IR alone increased the proportion of HeLa cells in the G2/M phase compared with controls, indicating activation of G2/M checkpoint in response to DNA damage. Although the combination of AM with IR did not further increase G2/M accumulation beyond IR alone, a significant reduction in the G0/G1 population was observed, suggesting preferential elimination of heavily damaged cells rather than prolonged cell cycle arrest, consistent with radiation-induced apoptotic cell loss and checkpoint-mediated elimination of irreparably damaged cells (115, 117, 118).

Apoptosis analysis further supported the radiosensitizing effects of AM, as the combination treatment markedly increased both early- and late-apoptotic cell populations compared with either AM or radiation alone. Apoptotic cell death represents a critical downstream outcome of excessive oxidative stress and persistent DNA damage (118). Previous studies have demonstrated that AM activates intrinsic apoptotic pathways through ROS-dependent mitochondrial dysfunction and activation of stress-responsive signaling cascades, including ASK1/p38 MAPK and caspase pathways (23, 101). These mechanisms provide a plausible explanation for the enhanced radiation-induced apoptosis observed in the present study. They are likely to contribute directly to the reduced clonogenic survival following combination treatment.

The functional consequence of these molecular and cellular events was ultimately confirmed by clonogenic survival analysis, which remains the gold standard for assessing long-term radiosensitivity (119). Combination treatment significantly reduced clonogenic survival to 28% compared with the control, whereas IR alone reduced survival to 62%, further supporting the radiosensitizing potential of AM. Importantly, severe DNA damage may result not only in apoptosis but also in reproductive cell death or mitotic catastrophe, in which cells may remain temporarily viable yet lose their long-term proliferative capacity (120, 121). This may explain why the IR group exhibited substantial γ-H2AX

induction but only a modest increase in apoptosis, while still showing a marked reduction in clonogenic survival. In contrast, AM alone, although inducing less DNA damage than IR, is known to promote ROS-dependent mitochondrial apoptosis (101), which may account for its relatively greater apoptotic effect despite lower γ-H2AX levels. Therefore, these findings are not contradictory but instead suggest that IR alone primarily compromises long-term reproductive survival, whereas AM more readily activates apoptotic signaling, and their combination intensifies both processes. In addition, at the same radiation dose of 2 Gy, the loss of clonogenic survival observed in the AM plus IR group was approximately 2.21-fold greater than that observed in the IR group, indicating that AM enhanced radiation-induced reproductive cell death. This finding highlights the radiosensitizing efficacy of AM and suggests that AM may enhance tumor cell killing when used in combination with IR, potentially allowing improved biological response at lower radiation doses. Since definitive RT for cervical cancer typically consists of pelvic external beam RT of about 45-50.4 Gy delivered in conventional 1.8-2 Gy fractions followed by brachytherapy (122), the ability of AM to enhance the biological effect at 2 Gy emphasizes its potential translational value as a natural radiosensitizer.

Taken together, these findings indicate that ionizing radiation serves as the primary inducer of DNA damage, whereas AM acts as a radiosensitizing agent that amplifies radiation-induced ROS, exacerbates DNA damage persistence, enhances G2/M cell cycle arrest, promotes apoptosis, and ultimately suppresses clonogenic survival. AM exhibits key characteristics of an effective radiosensitizer at sub-toxic concentrations and clinically relevant radiation doses. Although the present study was conducted in vitro, the mechanistic insights provided herein support further investigation of AM as a potential natural adjuvant to RT for cervical cancer in additional cellular models and in vivo systems.

CHAPTER VI

CONCLUSION

In conclusion, the present study demonstrates that AM enhances the radiosensitivity of cervical cancer (HeLa) cells at clinically relevant radiation doses. This radiosensitizing effect is associated with increased oxidative stress, persistent DNA damage, induced cell cycle arrest at G2/M phase, elevated apoptosis and suppression of clonogenic survival. Collectively, these findings support further investigation of AM as a potential natural radiosensitizer for RT.

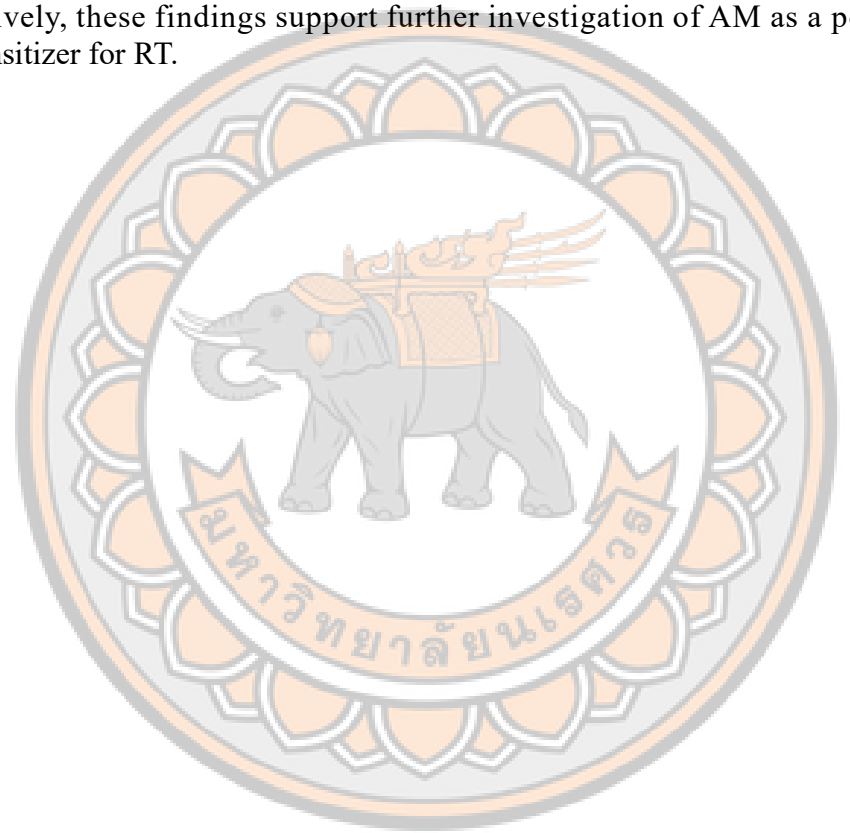

REFERENCES

REFERENCES

1. Bray F, Laversanne M, Sung H, Ferlay J, Siegel RL, Soerjomataram I, et al. Global cancer statistics 2022: GLOBOCAN estimates of incidence and mortality worldwide for 36 cancers in 185 countries. CA Cancer J Clin. 2024;74(3):229-63.
2. National Cancer Institute (Thailand). Hospital-based cancer registry 2021. Bangkok: National Cancer Institute; 2021.
3. Marth C, Landoni F, Mahner S, McCormack M, Gonzalez-Martin A, Colombo N. Cervical cancer: ESMO Clinical Practice Guidelines for diagnosis, treatment and follow-up. Ann Oncol. 2017;28(suppl_4):iv72-iv83.
4. Suh DH, Kim M, Kim HJ, Lee KH, Kim JW. Major clinical research advances in gynecologic cancer in 2015. J Gynecol Oncol. 2016;27(6):e53.
5. Tangjitgamol S, Levenback CF, Beller U, Kavanagh JJ. Role of surgical resection for lung, liver, and central nervous system metastases in patients with gynecological cancer: a literature review. Int J Gynecol Cancer. 2004;14(3):399-422.
6. Burmeister CA, Khan SF, Schäfer G, Mbatani N, Adams T, Moodley J, et al. Cervical cancer therapies: Current challenges and future perspectives. Tumour Virus Res. 2022;13:200238.
7. Begg AC, Stewart FA, Vens C. Strategies to improve radiotherapy with targeted drugs. Nat Rev Cancer. 2011;11(4):239-53.
8. Wang H, Mu X, He H, Zhang X-D. Cancer radiosensitizers. Trends Pharmacol Sci. 2018;39(1):24-48.
9. Amjad MT, Chidharla A, Kasi A. Cancer chemotherapy. *StatPearls*. Treasure Island (FL): StatPearls Publishing; 2026.
10. Mansoori B, Mohammadi A, Davudian S, Shirjang S, Baradaran B. The Different Mechanisms of Cancer Drug Resistance: A Brief Review. Adv Pharm Bull. 2017;7(3):339-48.
11. Weber GF. DNA damaging drugs. *Molecular therapies of cancer.* 2015. p. 9-112.
12. Adams GE. Chemical radiosensitization of hypoxic cells. Br Med Bull. 1973;29(1):48-53.
13. Fowler JF, Adams GE, Denekamp J. Radiosensitizers of hypoxic cells in solid tumours. Cancer Treat Rev. 1976;3(4):227-56.
14. Chendil D, Ranga RS, Meigooni D, Sathishkumar S, Ahmed MM. Curcumin confers radiosensitizing effect in prostate cancer cell line PC-3. Oncogene. 2004;23(8):1599-607.

15. Satish Rao BS, Sunil Kumar MR, Das S, Aithal K, Udupa N. Radiosensitizing potential of Plumbagin in B16F1 melanoma tumor cells through mitochondrial mediated programmed cell death. J Appl Biomed. 2015;13(4):279-88.

16. Shao Y, Quan F, Li HH, Yao XB, Zhao Q, Zhao RM. The radiosensitizing effect of resveratrol on hopypharyngeal carcinoma cell line FADU and its effect on the cell cycle. Zhong Xi Yi Jie He Xue Bao. 2015;35(6):699-703.

17. Petiwala SM, Li G, Ramaiya A, Kumar A, Gill RK, Saksena S, et al. Pharmacokinetic characterization of mangosteen (Garcinia mangostana) fruit extract standardized to α-mangostin in C57BL/6 mice. Nutr Res. 2014;34(4):336-45.

18. Alexandre J, Batteux F, Nicco C, Chéreau C, Laurent A, Guillevin L, et al. Accumulation of hydrogen peroxide is an early and crucial step for paclitaxel-induced cancer cell death both in vitro and in vivo. Int J Cancer. 2006;119(1):41-8.

19. Janhom P, Dharmasaroja P. Neuroprotective effects of alpha-mangostin on MPP(+)-induced apoptotic cell death in neuroblastoma SH-SY5Y cells. J Toxicol. 2015;2015:919058.

20. Lee YB, Ko KC, Shi MD, Liao YC, Chiang TA, Wu PF, et al. Alpha-mangostin, a novel dietary xanthone, suppresses TPA-mediated MMP-2 and MMP-9 expressions through the ERK signaling pathway in MCF-7 human breast adenocarcinoma cells. J Food Sci. 2010;75(1):H13-23.

21. Muchtaridi M, Wijaya C. Anticancer potential of α-mangostin. Asian J Pharm Clin Res. 2017;10:440.

22. Shih YW, Chien ST, Chen PS, Lee JH, Wu SH, Yin LT. Alpha-mangostin suppresses phorbol 12-myristate 13-acetate-induced MMP-2/MMP-9 expressions via alphavbeta3 integrin/FAK/ERK and NF-kappaB signaling pathway in human lung adenocarcinoma A549 cells. Cell Biochem Biophys. 2010;58(1):31-44.

23. Watanapokasin R, Jarinthanan F, Nakamura Y, Sawasjirakij N, Jaratrungtawee A, Suksamrarn S. Effects of α-mangostin on apoptosis induction of human colon cancer. World J Gastroenterol. 2011;17(16):2086-95.

24. El Habbash AI, Mohd Hashim N, Ibrahim MY, Yahayu M, Omer FAE, Abd Rahman M, et al. In vitro assessment of anti-proliferative effect induced by α-mangostin from Cratoxylum arborescens on HeLa cells. PeerJ. 2017;5:e3460.

25. de Martel C, Plummer M, Vignat J, Franceschi S. Worldwide burden of cancer attributable to HPV by site, country and HPV type. Int J Cancer. 2017;141(4):664-70.

26. Sahasrabuddhe VV. Cervical cancer: precursors and prevention. Hematol Oncol Clin North Am. 2024;38(4):771-81.

27. Stelzle D, Tanaka LF, Lee KK, Ibrahim Khalil A, Baussano I, Shah ASV, et al. Estimates of the global burden of cervical cancer associated with HIV. Lancet Glob Health. 2021;9(2):e161-e9.

28. Abboodi FF, Creek KE, Pirisi LA. Abstract LB-329: Molecular mechanisms of loss of E7 expression in HPV16-transformed human keratinocytes. Cancer Res. 2019;79(13 Suppl):LB-329.

29. McLaughlin-Drubin ME, Münger K. The human papillomavirus E7 oncoprotein. Virology. 2009;384(2):335-44.

30. Münger K, Baldwin A, Edwards KM, Hayakawa H, Nguyen CL, Owens M, et al. Mechanisms of human papillomavirus-induced oncogenesis. J Virol. 2004;78(21):11451-60.

31. Shai A, Nguyen ML, Wagstaff J, Jiang YH, Lambert PF. HPV16 E6 confers p53-dependent and p53-independent phenotypes in the epidermis of mice deficient for E6AP. Oncogene. 2007;26(23):3321-8.

32. Zhang W, Liu Y, Zhao N, Chen H, Qiao L, Zhao W, et al. Role of Cdk1 in the p53-independent abrogation of the postmitotic checkpoint by human papillomavirus E6. J Virol. 2015;89(5):2553-62.

33. Frazer I. Correlating immunity with protection for HPV infection. Int J Infect Dis. 2007;11 Suppl 2:S10-6.

34. Stanley M. HPV - immune response to infection and vaccination. Infect Agent Cancer. 2010;5:19.

35. Stanley M. Pathology and epidemiology of HPV infection in females. Gynecol Oncol. 2010;117(2):S5-S10.

36. Barakat R. Principles and practice of gynecologic oncology. Philadelphia, PA, USA. Lippincott Williams & Wilkins; 2009.

37. Berek JS, editor. Berek and Hacker's Gynecologic Oncology. 5th ed. Philadelphia, PA, USA: Lippincott Williams & Wilkins; 2009. 81-623 p.

38. Changede P. Staging of Cervical Cancer: What has Changed? J Obstet Gynaecol India. 2024;74(4):378-81.

39. Virarkar M, Vulasala SS, Morani A, Waters R, Gopireddy D, Kumar S, et al. Neuroendocrine Neoplasms of the Gynecologic Tract. Cancers. 2022;14:1835.

40. Bhatla N, Aoki D, Sharma DN, Sankaranarayanan R. Cancer of the cervix uteri. Int J Gynaecol Obstet. 2018;143 Suppl 2:22-36.

41. Jing H, Xiuhong W, Ying Y, Xiyun C, Deping L, Changmei S, et al. Complications of radical hysterectomy with pelvic lymph node dissection for cervical cancer: a 10-year single-centre clinical observational study. BMC Cancer. 2022;22(1):1286.

42. Koh WJ, Abu-Rustum NR, Bean S, Bradley K, Campos SM, Cho KR, et al. Cervical Cancer, Version 3.2019, NCCN Clinical Practice Guidelines in Oncology. J Natl Compr Canc Netw. 2019;17(1):64-84.

43. DeVita VT, Jr., Chu E. A history of cancer chemotherapy. Cancer Res. 2008;68(21):8643-53.

44. Coiffier B, Thieblemont C, Van Den Neste E, Lepeu G, Plantier I, Castaigne S, et al. Long-term outcome of patients in the LNH-98.5 trial, the first randomized study comparing rituximab-CHOP to standard CHOP chemotherapy in DLBCL patients: a study by the Groupe d'Etudes des Lymphomes de l'Adulte. Blood. 2010;116(12):2040-5.

45. Hudis CA. Trastuzumab — mechanism of action and use in clinical practice. N Engl J Med. 2007;357(1):39-51.

46. Partridge AH, Burstein HJ, Winer EP. Side effects of chemotherapy and combined chemohormonal therapy in women with early-stage breast cancer. JNCI Monogr. 2001;2001(30):135-42.

47. Housman G, Byler S, Heerboth S, Lapinska K, Longacre M, Snyder N, et al. Drug resistance in cancer: an overview. Cancers (Basel). 2014;6(3):1769-92.

48. Portelance L, Chao KSC, Grigsby PW, Bennet H, Low D. Intensity-modulated radiation therapy (IMRT) reduces small bowel, rectum, and bladder doses in patients with cervical cancer receiving pelvic and para-aortic irradiation. Int J Radiat Oncol Biol Phys. 2001;51(1):261-6.

49. Pötter R, Haie-Meder C, Limbergen EV, Barillot I, Brabandere MD, Dimopoulos J, et al. Recommendations from gynaecological (GYN) GEC ESTRO working group (II): concepts and terms in 3D image-based treatment planning in cervix cancer brachytherapy—3D dose volume parameters and aspects of 3D image-based anatomy, radiation physics, radiobiology. Radiother Oncol. 2006;78(1):67-77.

50. Bentzen SM, Constine LS, Deasy JO, Eisbruch A, Jackson A, Marks LB, et al. Quantitative Analyses of Normal Tissue Effects in the Clinic (QUANTEC): an introduction to the scientific issues. Int J Radiat Oncol Biol Phys. 2010;76(3 Suppl):S3-9.

51. Brown JM, Wilson WR. Exploiting tumour hypoxia in cancer treatment. Nat Rev Cancer. 2004;4(6):437-47.

52. Pinto F, Russo P. Brachytherapy: the urologist opinion. Urologia J. 2024;91(1):5-7.

53. Viswanathan AN, Creutzberg CL, Craighead P, McCormack M, Toita T, Narayan K, et al. International brachytherapy practice patterns: a survey of the gynecologic cancer intergroup (GCIG). Int J Radiat Oncol Biol Phys. 2012;82(1):250-5.

54. Galluzzi L, Vitale I, Aaronson SA, Abrams JM, Adam D, Agostinis P, et al. Molecular mechanisms of cell death: recommendations of the Nomenclature Committee on Cell Death 2018. Cell Death Differ. 2018;25(3):486-541.

55. Majno G, Joris I. Apoptosis, oncosis, and necrosis. An overview of cell death. Am J Pathol. 1995;146(1):3-15.

56. Shen S, Shao Y, Li C. Different types of cell death and their shift in shaping disease. Cell Death Discov. 2023;9.

57. Zhu X, Li S. Ferroptosis, necroptosis, and pyroptosis in gastrointestinal cancers: the chief culprits of tumor progression and drug resistance. Adv Sci. 2023;10.

58. Azzam EI, Jay-Gerin JP, Pain D. Ionizing radiation-induced metabolic oxidative stress and prolonged cell injury. Cancer Lett. 2012;327(1-2):48-60.

59. Jay-Gerin J-P. Fundamentals of water radiolysis. Encyclopedia. 2025;5(1):38.

60. Srinivas US, Tan BWQ, Vellayappan BA, Jeyasekharan AD. ROS and the DNA damage response in cancer. Redox Biol. 2019;25:101084.

61. Kowalczyk P, Sulejczak D, Kleczkowska P, Bukowska-Ośko I, Kucia M, Popiel M, et al. Mitochondrial oxidative stress-a causative factor and therapeutic target in many diseases. Int J Mol Sci. 2021;22(24).

62. Meng L, Liu S, Luo J, Tu Y, Li T, Li P, et al. Oxidative stress and reactive oxygen species in otorhinolaryngological diseases: insights from pathophysiology to targeted antioxidant therapies. Redox Rep. 2025;30(1):2458942.

63. Bayir H, Kagan VE. Bench-to-bedside review: Mitochondrial injury, oxidative stress and apoptosis--there is nothing more practical than a good theory. Crit Care. 2008;12(1):206.

64. Gu JJ, Kaufman GP, Mavis C, Czuczman MS, Hernandez-Ilizaliturri FJ. Mitotic catastrophe and cell cycle arrest are alternative cell death pathways executed by bortezomib in rituximab resistant B-cell lymphoma cells. Oncotarget. 2017;8(8):12741-53.

65. Kuczler MD, Olseen AM, Pienta KJ, Amend SR. ROS-induced cell cycle arrest as a mechanism of resistance in polyaneuploid cancer cells (PACCs). Prog Biophys Mol Biol. 2021;165:3-7.

66. Howard D, Sebastian S, Le QV-C, Thierry B, Kempson I. Chemical mechanisms of nanoparticle radiosensitization and radioprotection: a review of structure-function relationships influencing reactive oxygen species. Int J Mol Sci. 2020;21(2):579.

67. Mah LJ, Orlowski C, Ververis K, Vasireddy RS, El-Osta A, Karagiannis TC. Evaluation of the efficacy of radiation-modifying compounds using γH2AX as a molecular marker of DNA double-strand breaks. Genome Integr. 2011;2(1):3.

68. Podhorecka M, Skladanowski A, Bozko P. H2AX phosphorylation: its role in DNA damage response and cancer therapy. J Nucleic Acids. 2010;2010.

69. Venkatesulu BP, Krishnan S. Radiosensitization by inhibiting DNA repair: turning the spotlight on homologous recombination. Hepatology. 2018;67(2):470-2.

70. Stupp R, Mason WP, MJvd B, Weller M, Fisher B, Taphoorn MJB, et al. Radiotherapy plus concomitant and adjuvant temozolomide for glioblastoma. N Engl J Med. 2005;352(10):987-96.

71. Bernier J, Domenge C, Ozsahin M, Matuszewska K, Lefebvre J-L, Greiner RH, et al. Postoperative irradiation with or without concomitant chemotherapy for locally advanced head and neck cancer. N Engl J Med. 2004;350(19):1945-52.

72. Keys HM, Bundy BN, Stehman FB, Muderspach LI, Chafe WE, Suggs CL, et al. Cisplatin, radiation, and adjuvant hysterectomy compared with radiation and adjuvant hysterectomy for bulky stage IB cervical carcinoma. N Engl J Med. 1999;340(15):1154-61.

73. Maier P, Hartmann L, Wenz F, Herskind C. Cellular pathways in response to ionizing radiation and their targetability for tumor radiosensitization. Int J Mol Sci. 2016;17(1).

74. Schuemann J, Bagley AF, Berbeco R, Bromma K, Butterworth KT, Byrne HL, et al. Roadmap for metal nanoparticles in radiation therapy: current status, translational challenges, and future directions. Phys Med Biol. 2020;65(21):21rm02.

75. McMahon SJ, Hyland WB, Muir MF, Coulter JA, Jain S, Butterworth KT, et al. Nanodosimetric effects of gold nanoparticles in megavoltage radiation therapy. Radiother Oncol. 2011;100(3):412-6.

76. Lin Y, McMahon SJ, Paganetti H, Schuemann J. Biological modeling of gold nanoparticle enhanced radiotherapy for proton therapy. Phys Med Biol. 2015;60(10):4149.

77. Dayal R, Singh A, Pandey A, Mishra KP. Reactive oxygen species as mediator of tumor radiosensitivity. J Cancer Res Ther. 2014;10(4):811-8.

78. Nickoloff J, Jones D, Lee S-H, Williamson E, Hromas R. Drugging the cancers addicted to DNA repair. JNCI J Natl Cancer Inst. 2017;109.

79. Vignard J, Mirey G, Salles B. Ionizing-radiation induced DNA double-strand breaks: a direct and indirect lighting up. Radiother Oncol. 2013;108(3):362-9.

80. Baskar R, Lee KA, Yeo R, Yeoh KW. Cancer and radiation therapy: current advances and future directions. Int J Med Sci. 2012;9(3):193-9.

81. Tishler RB, Geard CR, Hall EJ, Schiff PB. Taxol sensitizes human astrocytoma cells to radiation. Cancer Res. 1992;52(12):3495-7.

82. Ghafouri-Fard S, Abak A, Tondro Anamag F, Shoorei H, Fattahi F, Javadinia SA, et al. 5-fluorouracil: a narrative review on the role of regulatory mechanisms in driving resistance to this chemotherapeutic agent. Front Oncol. 2021;11:658636.

83. Crane CH, Skibber JM, Birnbaum EH, Feig BW, Singh AK, Delclos ME, et al. The addition of continuous infusion 5-FU to preoperative radiation therapy increases tumor response, leading to increased sphincter preservation in locally advanced rectal cancer. Int J Radiat Oncol Biol Phys. 2003;57(1):84-9.

84. Zhang J, Stevens M, Bradshaw T. Temozolomide: mechanisms of action, repair and resistance. Curr Mol Pharmacol. 2011;5:102-14.

85. Nisar S, Masoodi T, Prabhu KS, Kuttikrishnan S, Zarif L, Khatoon S, et al. Natural products as chemo-radiation therapy sensitizers in cancers. Biomed Pharmacother. 2022;154:113610.

86. Fan H, Shao M, Huang S, Liu Y, Liu J, Wang Z, et al. miR-593 mediates curcumin-induced radiosensitization of nasopharyngeal carcinoma cells via MDR1. Oncol Lett. 2016;11(6):3729-34.

87. Wang Q, Fan H, Liu Y, Yin Z, Cai H, Liu J, et al. Curcumin enhances the radiosensitivity in nasopharyngeal carcinoma cells involving the reversal of differentially expressed long non-coding RNAs. Int J Oncol. 2014;44(3):858-64.

88. Xu R, Li H, Wu S, Qu J, Yuan H, Zhou Y, et al. MicroRNA-1246 regulates the radio-sensitizing effect of curcumin in bladder cancer cells via activating P53. Int Urol Nephrol. 2019;51(10):1771-9.

89. Liu G, Wang Y, Li M. Curcumin sensitized the antitumour effects of irradiation in promoting apoptosis of oesophageal squamous-cell carcinoma through NF-κB signalling pathway. J Pharm Pharmacol. 2018;70(10):1340-8.

90. Nair S, Nair RR, Srinivas P, Srinivas G, Pillai MR. Radiosensitizing effects of plumbagin in cervical cancer cells is through modulation of apoptotic pathway. Mol Carcinog. 2008;47(1):22-33.

91. Prasad VS, Devi PU, Rao B, Kamath R. Radiosensitizing effect of plumbagin on mouse melanoma cells grown in vitro. Indian J Exp Biol. 1996;34(9):857-8.

92. Chen Y-A, Lien H-M, Kao M-C, Lo UG, Lin L-C, Lin C-J, et al. Sensitization of radioresistant prostate cancer cells by resveratrol isolated from Arachis hypogaea stems. PLoS One. 2017;12(1):e0169204.

93. da Costa Araldi IC, Bordin FPR, Cadoná FC, Barbisan F, Azzolin VF, Teixeira CF, et al. The in vitro radiosensitizer potential of resveratrol on MCF-7 breast cancer cells. Chem Biol Interact. 2018;282:85-92.

94. Kao C-L, Huang P-I, Tsai P-H, Tsai M-L, Lo J-F, Lee Y-Y, et al. Resveratrol-induced apoptosis and increased radiosensitivity in CD133-positive cells derived from atypical teratoid/rhabdoid tumor. Int J Radiat Oncol Biol Phys. 2009;74(1):219-28.

95. Tan Y, Wei X, Zhang W, Wang X, Wang K, Du B, et al. Resveratrol enhances the radiosensitivity of nasopharyngeal carcinoma cells by downregulating E2F1. Oncol Rep. 2017;37(3):1833-41.

96. Ji X, Avula B, Khan IA. Quantitative and qualitative determination of six xanthones in Garcinia mangostana L. by LC-PDA and LC-ESI-MS. J Pharm Biomed Anal. 2007;43 (4):1270-6.

97. Pedraza-Chaverri J, Cardenas N, Orozco-Ibarra M, Pérez-Rojas J. Medicinal properties of mangosteen (Garcinia mangostana). Food Chem Toxicol. 2008;46:3227-39.

98. Li P, Tian W, Ma X. Alpha-mangostin inhibits intracellular fatty acid synthase and induces apoptosis in breast cancer cells. Mol Cancer. 2014;13(1):138.

99. Phan TKT, Shahbazzadeh F, Pham TTH, Kihara T. Alpha-mangostin inhibits the migration and invasion of A549 lung cancer cells. PeerJ. 2018;6:e5027.

100. Johnson JJ, Petiwala SM, Syed DN, Rasmussen JT, Adhami VM, Siddiqui IA, et al. α-Mangostin, a xanthone from mangosteen fruit, promotes cell cycle arrest in prostate cancer and decreases xenograft tumor growth. Carcinogenesis. 2012;33(2):413-9.

101. Lee C-H, Ying T-H, Chiou H-L, Hsieh S-C, Wen S-H, Chou R-H, et al. Alpha-mangostin induces apoptosis through activation of reactive oxygen species and ASK1/p38 signaling pathway in cervical cancer cells. Oncotarget. 2017;8(29).

102. Aisha AF, Abu-Salah KM, Ismail Z, Majid AM. In vitro and in vivo anti-colon cancer effects of Garcinia mangostana xanthones extract. BMC Complement Altern Med. 2012;12:104.

103. Pedraza-Chaverri J, Cárdenas-Rodríguez N, Orozco-Ibarra M, Pérez-Rojas JM. Medicinal properties of mangosteen (Garcinia mangostana). Food Chem Toxicol. 2008;46(10):3227-39.

104. Cruz-Gregorio A, Aranda-Rivera AK, Aparicio-Trejo OE, Medina-Campos ON, Sciutto E, Fragoso G, et al. α-Mangostin induces oxidative damage, mitochondrial dysfunction, and apoptosis in a triple-negative breast cancer model. Phytother Res. 2023;37(8):3394-407.

105. Hunting D, Gantchev T. DNA radiosensitization: the search for repair refractive lesions including double strand breaks and interstrand crosslinks. In: Chen CC, editor. *Selected Topics in DNA Repair*. London: IntechOpen; 2011.

106. Gong L, Zhang Y, Liu C, Zhang M, Han S. Application of radiosensitizers in cancer radiotherapy. Int J Nanomedicine. 2021;16:1083-102.

107. Wang W, Yu Z, Su W. Ion irradiation and biomolecular radiation damage II. Indirect effect. arXiv [preprint, biological physics]. 2010.

108. Komorowska D, Radzik T, Kalenik S, Rodacka A. Natural radiosensitizers in radiotherapy: cancer treatment by combining ionizing radiation with resveratrol. Int J Mol Sci. 2022;23(18).

109. Dayal R, Singh A, Pandey A, Mishra KP. Reactive oxygen species as mediator of tumor radiosensitivity. J Cancer Res Ther. 2014;10(4):811-8.

110. Celeste A, Fernandez-Capetillo O, Kruhlak MJ, Pilch DR, Staudt DW, Lee A, et al. Histone H2AX phosphorylation is dispensable for the initial recognition of DNA breaks. Nat Cell Biol. 2003;5(7):675-9.

111. Mladenov E, Magin S, Soni A, Iliakis G. DNA double-strand break repair as determinant of cellular radiosensitivity to killing and target in radiation therapy. Front Oncol. 2013;3:113.

112. Mah LJ, Vasireddy RS, Tang MM, Georgiadis GT, El-Osta A, Karagiannis TC. Quantification of γH2AX foci in response to ionizing radiation. J Vis Exp. 2010(38).

113. Dukaew N, Konishi T, Chairatvit K, Autsavapromporn N, Soonthornchareonnon N, Wongnoppavich A. Enhancement of radiosensitivity by eurycomalactone in human NSCLC cells through G_2/M cell cycle arrest and delayed DNA double-strand break repair. Oncol Res. 2020;28(2):161-75.

114. Mladenov E, Iliakis G. Induction and repair of DNA double strand breaks: the increasing spectrum of non-homologous end joining pathways. Mutat Res. 2011;711(1-2):61-72.

115. Kastan MB, Bartek J. Cell-cycle checkpoints and cancer. Nature. 2004;432(7015):316-23.

116. Sia J, Szmyd R, Hau E, Gee HE. Molecular mechanisms of radiation-induced cancer cell death: a primer. Front Cell Dev Biol. 2020;8:41.

117. Pawlik TM, Keyomarsi K. Role of cell cycle in mediating sensitivity to radiotherapy. Int J Radiat Oncol Biol Phys. 2004;59(4):928-42.

118. Eriksson D, Stigbrand T. Radiation-induced cell death mechanisms. Tumour Biol. 2010;31(4):363-72.

119. Fertil B, Malaise EP. Intrinsic radiosensitivity of human cell lines is correlated with radioresponsiveness of human tumors: analysis of 101 published survival curves. Int J Radiat Oncol Biol Phys. 1985;11(9):1699-707.

120. Sazonova EV, Petrichuk SV, Kopeina GS, Zhivotovsky B. A link between mitotic defects and mitotic catastrophe: detection and cell fate. Biol Direct. 2021;16(1):25.

121. Zhang Z, Yang J, Maimaitiyimin R, Ma M, Zhang H, Wang R. Radiation-induced mitotic catastrophe is associated with down-regulated ribosomal biosynthesis and mitosis genes. All Life. 2020;13:474-85.

122. Fu Q, Li W, Zuo J, Yang X, Xu Y, Huang M, et al. A feasibility study of a modified treatment strategy combined external beam radiation therapy and brachytherapy for cervical cancer. J Appl Clin Med Phys. 2022;23(7):e13621.

APPENDIX

APPENDIX A Summary of cytotoxicity of AM in HeLa cells at 24 hours.

Table A cytotoxicity of Alpha-Mangostin in HeLa cells after 24 hours treatment assessed by MTT assay (n=3).

Alpha-Mangostin (μM)	% Cell viability
	100.00
0	100.00
	100.00
Average	**100.00**
SD	**0.00**
	98.00
5	98.00
	98.00
Average	**98.00**
SD	**0.00**
	92.11
10	91.30
	89.95
Average	**91.12**
SD	**1.09**
15	68.80
	69.67
	75.56
Average	**71.35**
SD	**3.68**
20	51.54
	50.08
	53.68
Average	**51.77**
SD	**1.81**

Table A cytotoxicity of Alpha-Mangostin in HeLa cells after 24 hours treatment assessed by MTT assay (n=3) (continued).

Alpha-Mangostin (µM)	% Cell viability
25	27.89
	24.56
	23.34
Average	**25.27**
SD	**2.35**
30	12.70
	16.73
	13.62
Average	**14.35**
SD	**2.11**
35	6.29
	6.78
	6.07
Average	**6.38**
SD	**0.36**

APPENDIX B Summary of cytotoxicity of AM in fibroblast cells at 24 hours.

Table B cytotoxicity of Alpha-Mangostin in Fibroblast cells after 24 hours treatment assessed by MTT assay (n=3).

Alpha-Mangostin (μM)	% Cell viability
	100.00
0	100.00
	100.00
Average	**100.00**
SD	**0.00**
	119.61
5	100.20
	98.14
Average	**105.98**
SD	**11.85**
	109.16
10	11.56
	102.75
Average	**107.82**
SD	**4.55**
15	91.99
	79.92
	108.29
Average	**93.40**
SD	**14.24**
20	108.62
	106.45
	87.74
Average	**100.94**
SD	**11.48**

Table B cytotoxicity of Alpha-Mangostin in Fibroblast cells after 24 hours treatment assessed by MTT assay (n=3) (continued).

Alpha-Mangostin (µM)	% Cell viability
25	85.90
	79.59
	91.66
Average	**85.72**
SD	**6.04**
30	40.88
	43.38
	40.23
Average	**41.50**
SD	**1.66**
35	35.55
	51.10
	32.51
Average	**39.72**
SD	**9.97**

APPENDIX C Summary of radiation lethal dose determination in HeLa cells.

Table C radiation lethal dose determination in HeLa cells assessed by Clonogenic survival assay (n=3).

Radiation dose (Gy)	SF
	1.00
0	1.00
	1.00
Average	**1.00**
SD	**0.00**
	0.99
1	0.88
	1.02
Average	**0.96**
SD	**0.07**
	0.65
2	0.64
	0.68
Average	**0.66**
SD	**0.02**
4	0.35
	0.35
	0.34
Average	**0.35**
SD	**0.01**
6	0.20
	0.25
	0.26
Average	**0.23**
SD	**0.03**

APPENDIX D Intercellular reactive oxygen species (ROS) levels in HeLa cells under different treatment conditions assessed by H_2DCFDA assay

Table D Relative fluorescence intensity of intercellular ROS in HeLa cells under different treatment conditions (n=3).

Conditions	Relative Fluorescence Intensity
Control	1.00
	1.00
	1.00
Average	**1.00**
SD	**0.00**
AM	1.18
	1.08
	1.12
Average	**0.05**
SD	**0.07**
2 Gy	3.47
	3.17
	3.33
Average	**3.32**
SD	**0.15**
AM+2 Gy	4.24
	3.89
	4.08
Average	**4.07**
SD	**0.18**

APPENDIX E Quantification of γ-H2AX immunofluorescence intensity assessed by γ-H2AX Immunofluorescence Assay

Table E Individual field of view fluorescence intensity values and calculated % γ-H2AX/DAPI in HeLa cells under different treatment conditions (n=5).

Conditions	Replicates	Mean intensity		% yH2AX/DAPI
		DAPI	yH2AX	
Control	n1	35.837	0.21	0.59
	n2	66.376	0.45	0.68
	n3	30.439	0.17	0.56
	n4	25.341	0.203	0.80
	n5	32.306	0.229	0.71
	Average			**0.67**
	SD			**0.10**
AM	n1	35.293	3.732	10.57
	n2	52.241	6.132	11.74
	n3	45.013	5.507	12.23
	n4	33.61	4.998	14.87
	n5	48.176	5.724	11.88
	Average			**12.26**
	SD			**1.59**
2 Gy	n1	47.218	12.193	25.82
	n2	42.574	10.865	25.52
	n3	51.028	12.421	24.34
	n4	52.189	14.894	28.54
	n5	60.565	15.43	25.48
	Average			**25.94**
	SD			**1.56**

Table E Individual field of view fluorescence intensity values and calculated % γ-H2AX/DAPI in HeLa cells under different treatment conditions (n=5) (continued).

Conditions	Replicates	Mean intensity		% yH2AX/DAPI
		DAPI	yH2AX	
AM+2 Gy	n1	45.685	26.414	57.82
	n2	53.804	25.464	47.33
	n3	32.49	16.383	50.42
	n4	39.254	17.875	45.54
	n5	34.524	13.775	39.90
	Average			**48.20**
	SD			**6.60**

APPENDIX F Cell cycle analysis in HeLa cells determined by Muse® Cell Cycle Kit

Table F Percentage of cell cycle distribution of HeLa cells under different treatment conditions (n=5).

Conditions	Percentage of cell cycle distribution			
	G0/G1	**S**	**G2/M**	**Debris**
Control	75.10	8.10	14.90	38.10
	71.4	13.7	13.6	32.5
	70.10	16.40	13.50	53.70
	70.1	12.8	17.1	87.6
	69.4	18.30	11.80	40.60
Average	**71.22**	**13.86**	**14.18**	**50.50**
SD	**2.29**	**3.89**	**1.97**	**22.15**
AM	64.00	15.60	20.40	24.70
	59.40	17.50	23.00	30.50
	61.2	14.1	21.1	59.1
	60	20.3	19.3	47.6
	59.2	19	21.7	84.6
Average	**60.76**	**17.30**	**21.10**	**49.30**
SD	**1.97**	**2.50**	**1.39**	**24.00**
2 Gy	57.2	17.3	21.7	73.3
	61.90	17.10	20.40	49.90
	65.2	14.4	20.4	78.3
	61.3	17.8	20.8	83.5
	54.5	20.9	22.8	45.2
Average	**60.02**	**17.50**	**21.22**	**66.04**
SD	**4.20**	**2.32**	**1.03**	**17.34**

Table F Percentage of cell cycle distribution of HeLa cells under different treatment conditions (n=5) (continued).

Conditions	Percentage of cell cycle distribution			
	G0/G1	**G0/G1**	**G0/G1**	**G0/G1**
AM+2 Gy	57.25	13	23.6	44.2
	49.4	18.1	31.7	59.1
	48.8	26.7	24.5	91.3
	54.2	18.7	26.9	90.1
	50.4	22.3	26.6	45
Average	**52.01**	**19.76**	**26.66**	**65.94**
SD	**3.60**	**5.10**	**3.14**	**23.37**

APPENDIX G Apoptosis analysis in HeLa cells determined by Muse® Annexin V & Dead Cell Kit.

Table G Percentage of live, early apoptotic, late apoptotic, total apoptotic, and dead HeLa cells under different treatment conditions (n=5).

Conditions	% of cell (cells/ml)				
	Live	Early apoptotic	Late apoptotic	Total apoptotic	Dead
Control	97.23	0.50	2.21	2.71	0.05
	98.69	0.38	0.79	1.17	0.14
	98.06	0.71	1.20	1.91	0.04
	92.49	5.28	2.23	7.51	0.00
	93.17	4.24	2.56	6.80	0.03
Average	**95.93**	**2.22**	**1.80**	**4.02**	**0.05**
SD	**2.89**	**2.35**	**0.76**	**2.92**	**0.05**
AM	77.01	20.47	2.30	22.77	0.22
	79.72	17.85	2.36	20.21	0.06
	76.83	20.30	2.38	22.68	0.50
	74.64	12.52	12.88	25.40	0.00
	81.59	11.45	6.89	18.34	0.07
Average	**77.96**	**16.52**	**5.36**	**21.88**	**0.17**
SD	**2.71**	**4.28**	**4.64**	**2.70**	**0.20**
2 Gy	97.32	0.52	2.16	2.68	0.00
	94.55	1.14	4.13	5.27	0.18
	91.27	8.56	0.16	8.72	0.00
	91.76	7.94	0.24	8.18	0.02
	89.04	8.23	2.71	10.94	0.02
Average	**92.79**	**5.28**	**1.88**	**7.16**	**0.04**
SD	**2.87**	**3.64**	**1.52**	**2.88**	**0.07**

Table G Percentage of live, early apoptotic, late apoptotic, total apoptotic, and dead HeLa cells under different treatment conditions (n=5) (continued).

Conditions	% of cell (cells/ml)				
	Live	Early apoptotic	Late apoptotic	Total apoptotic	Dead
AM+2 Gy	69.68	27.28	2.76	30.04	0.28
	55.89	34.63	9.35	43.98	0.13
	59.12	25.06	15.57	40.63	0.25
	47.17	47.65	5.15	52.80	0.03
	70.04	23.90	6.04	29.94	0.02
Average	**60.38**	**31.70**	**7.77**	**39.48**	**0.14**
SD	**9.70**	**9.84**	**4.96**	**9.74**	**0.12**

APPENDIX H Clonogenic survival data of HeLa cells.

Table H Individuals SF values of HeLa cells under different treatment conditions (n=5).

Conditions	SF
Control	1.00
	1.00
	1.00
	1.00
	1.00
Average	**1.00**
SD	**0.00**
AM	0.68
	0.77
	0.71
	0.89
	0.88
Average	**0.79**
SD	**0.10**
2 Gy	0.51
	0.72
	0.67
	0.52
	0.7
Average	**0.62**
SD	**0.10**

Table H Individuals SF values of HeLa cells under different treatment conditions (n=5) (continued).

Conditions	SF
AM+2 Gy	0.16
	0.28
	0.31
	0.37
	0.27
Average	**0.28**
SD	**0.08**

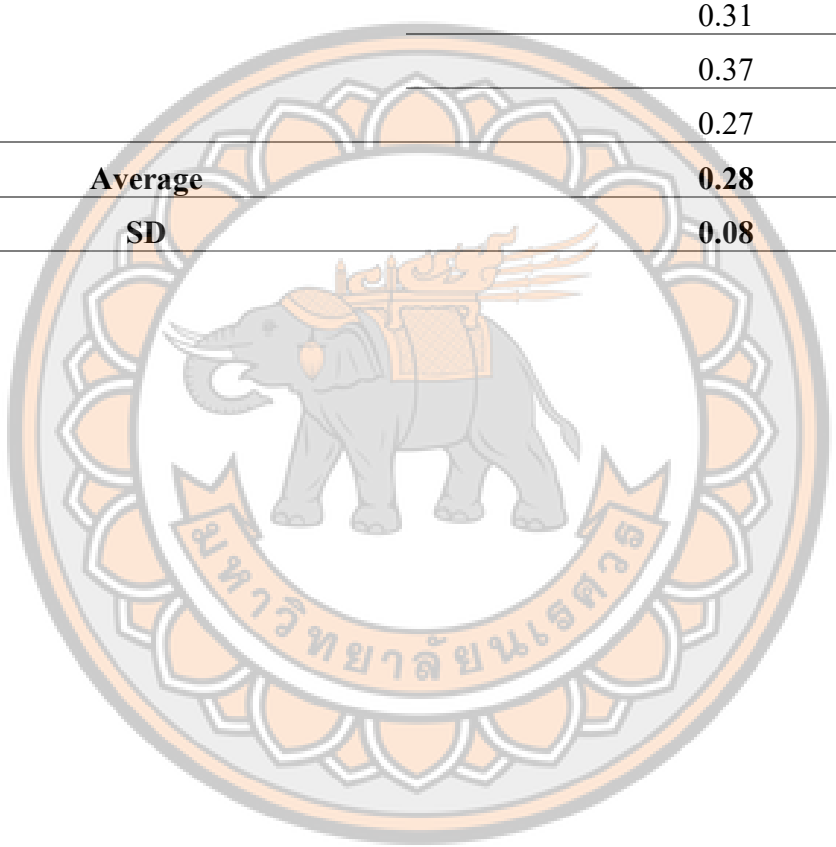

APPENDIX I Certificate of Approval Biosafety and Biosecurity.

ใบรับรองด้านความปลอดภัยทางชีวภาพ

ชื่อโครงการ (ภาษาไทย)	ผลการเพิ่มความไวต่อรังสีของสารแอลฟา-แมงโกสทินในเซลล์มะเร็งปากมดลูก (ฮีล่า)
ชื่อโครงการ (ภาษาอังกฤษ)	Radiosensitization Effect of Alpha-Mangostin on Cervical Cancer (HeLa) Cells
ชื่อโครงการย่อย/กิจกรรมที่เกี่ยวข้องกับความปลอดภัยทางชีวภาพ (กรณีเป็นเพียงส่วนหนึ่งของชุดโครงการ/โครงการ)	-
ชื่อผู้ขอรับการรับรองฯ	นางสาวพิมพ์วรีย์ อิศรา
ชื่ออาจารย์ที่ปรึกษา	ผู้ช่วยศาสตราจารย์ ดร.อัศนัย ประพันธ์
สังกัดหน่วยงาน/คณะ	คณะสหเวชศาสตร์
เลขสำคัญโครงการ	NUIBC OT 68-04-22
เลขที่รับรองโครงการ	68-33
ประเภทการรับรอง	งานวิจัยประเภทที่ 2
การรับรองครั้งที่ 1	แบบเสนอเพื่อขอรับการพิจารณารับรองด้านความปลอดภัยทางชีวภาพนี้ ได้ผ่านการพิจารณาและรับรองจากคณะกรรมการควบคุมความปลอดภัยทางชีวภาพ มหาวิทยาลัยนเรศวร ครั้งที่ 11/2568 เมื่อวันที่ 6 สิงหาคม 2568 เห็นว่ามีความสอดคล้องกับแนวทางปฏิบัติเพื่อความปลอดภัยทางชีวภาพ จึงเห็นควรให้ดำเนินการวิจัยด้านความปลอดภัยทางชีวภาพตามข้อเสนอการวิจัยนี้ได้
วันหมดอายุครั้งที่ 1	5 สิงหาคม 2569

ลงนาม

(ดร.วิสาข์ สุพรรณไพบูลย์)

ประธานคณะกรรมการควบคุมความปลอดภัยทางชีวภาพ

มหาวิทยาลัยนเรศวร

หมายเหตุ ใบรับรองฉบับนี้ใช้ควบคู่กับหนังสือราชการ เลขที่ อว 0603.01.13(1)/ว 2309 ลงวันที่ 13 สิงหาคม 2568

Figure 21 Certificate of Approval Biosafety and Biosecurity conducted by Naresuan University